Title

Appropriately differentiated ARPE-19 cells regain phenotype and gene expression profiles similar to those of native RPE cells.

Authors

Samuel, William
Jaworski, Cynthia
Postnikova, Olga A
et al.

Publication Date

2017

Peer reviewed

Molecular Vision 2017; 23:60-89 <http://www.molvis.org/molvis/v23/60>
Received 20 June 2016 | Accepted 3 March 2017 | Published 5 March 2017

Appropriately differentiated ARPE-19 cells regain phenotype and gene expression profiles similar to those of native RPE cells

William Samuel,[1] Cynthia Jaworski,[1] Olga. A. Postnikova,[1] R. Krishnan Kutty,[1] Todd Duncan,[1] Li Xuan Tan,[2] Eugenia Poliakov,[1] Aparna Lakkaraju,[2] T. Michael Redmond[1]

[1]Laboratory of Retinal Cell and Molecular Biology, National Eye Institute, National Institutes of Health, Bethesda, MD; [2]Department of Ophthalmology and Visual Sciences, School of Medicine and Public Health, University of Wisconsin-Madison, Madison, WI

Purpose: The RPE cell line ARPE-19 provides a dependable and widely used alternative to native RPE. However, replication of the native RPE phenotype becomes more difficult because these cells lose their specialized phenotype after multiple passages. Compounding this problem is the widespread use of ARPE-19 cells in an undifferentiated state to attempt to model RPE functions. We wished to determine whether suitable culture conditions and differentiation could restore the RPE-appropriate expression of genes and proteins to ARPE-19, along with a functional and morphological phenotype resembling native RPE. We compared the transcriptome of ARPE-19 cells kept in long-term culture with those of primary and other human RPE cells to assess the former's inherent plasticity relative to the latter.

Methods: ARPE-19 cells at passages 9 to 12 grown in DMEM containing high glucose and pyruvate with 1% fetal bovine serum were differentiated for up to 4 months. Immunocytochemistry was performed on ARPE-19 cells grown on filters. Total RNA extracted from ARPE-19 cells cultured for either 4 days or 4 months was used for RNA sequencing (RNA-Seq) analysis using a 2 × 50 bp paired end protocol. The RNA-Seq data were analyzed to identify the affected pathways and recognize shared ontological classification among differentially expressed genes. RPE-specific mRNAs and miRNAs were assessed with quantitative real-time (RT)–PCR, and proteins with western blotting.

Results: ARPE-19 cells grown for 4 months developed the classic native RPE phenotype with heavy pigmentation. RPE-expressed genes, including *RPE65*, *RDH5*, and *RDH10*, as well as miR-204/211, were greatly increased in the ARPE-19 cells maintained at confluence for 4 months. The RNA-Seq analysis provided a comprehensive view of the relative abundance and differential expression of the genes in the differentiated ARPE-19 cells. Of the 16,757 genes with detectable signals, nearly 1,681 genes were upregulated, and 1,629 genes were downregulated with a fold change of 2.5 or more differences between 4 months and 4 days of culture. Gene Ontology analysis showed that the upregulated genes were associated with visual cycle, phagocytosis, pigment synthesis, cell differentiation, and RPE-related transcription factors. The majority of the downregulated genes play a role in cell cycle and proliferation.

Conclusions: The ARPE-19 cells cultured for 4 months developed a phenotype characteristic of native RPE and expressed proteins, mRNAs, and miRNAs characteristic of the RPE. Comparison of the ARPE-19 RNA-Seq data set with that of primary human fetal RPE, embryonic stem cell–derived RPE, and native RPE revealed an important overall similar expression ratio among all the models and native tissue. However, none of the cultured models reached the absolute values in the native tissue. The results of this study demonstrate that low-passage ARPE-19 cells can express genes specific to native human RPE cells when appropriately cultured and differentiated.

The RPE, a polarized monolayer of highly differentiated epithelial cells, positioned strategically between the neural retina and the vascular choriocapillaris, performs crucial functions that are necessary to maintain the function and survival of the photoreceptors and other retinal cells. These functions include the formation of the blood–retinal barrier by tight junctions, transporting nutrients to the neural retina, regulating ion, pH, and fluid homeostasis in the subretinal space, absorbing excess light, scavenging free radicals and reactive oxygen species (ROS), regenerating the visual chromophore 11-*cis* retinal, and phagocytosing and degrading rod outer segments that are undergoing circadian shedding [1]. Because of these functions, the integrity of the RPE is critical for retinal function, and damage or malfunction of the RPE may play a central role in the pathogenesis of various retinal diseases, such as retinitis pigmentosa and age-related macular degeneration (AMD) [2,3].

In vitro cultures of human RPE cells present an attractive model for studying the physiology and pathophysiology of native tissue. Although much work has been done using immortalized cell lines created from several species, including the rat, pig, and human [4-6], these RPE culture models generally fail to preserve many of their specialized characteristics and the ability to recapitulate functional

Correspondence to: William Samuel, LRCMB, Bldg 6/ Room 112A, National Eye Institute, National Institutes of Health, 6 Center Drive, Bethesda, Maryland 20892-0608; Phone: (301) 402-5367; FAX: (301) 402-1883; email: samuelw@nei.nih.gov

characteristics and gene expression patterns exhibited by the RPE in vivo. Primary cultures of human fetal RPE (fhRPE) have been used widely as they are known to retain many characteristics of the native human RPE [7-9], while primary cultures of the adult human RPE are considered the most physiologically mature form to study RPE in vitro [10]. However, primary RPE cells cultured from different donors may exhibit physiological differences and lose their capacity to redifferentiate after a limited number of expansions, also losing important RPE characteristics [11]. An important disadvantage of culturing human primary RPE cells is that human eyes are often difficult to obtain. Another disadvantage is the genetic variability inherent in the use of cells from different donors.

ARPE-19, a human RPE cell line established by Dunn et al. [5] from a single individual, has been used as an alternative to native RPE as these cells exhibit epithelial cell morphology and express several genes specific for the RPE, such as RPE65, a protein preferentially and abundantly expressed in the RPE [12], and cellular retinaldehyde-binding protein (CRALBP), a retinoid-binding protein involved in the regeneration of visual pigment [13]. These cells perform many of the known functions of the human RPE, including assimilation of photoreceptor outer segments (POS) by phagocytosis [5,14]. In addition, these cells have been widely used to study various aspects of cell growth and differentiation [15-18]. However, it has become difficult to replicate some differentiated characteristics of the native RPE because ARPE-19 cells lose their specialized properties after multiple passages. Epithelial-mesenchymal transition (EMT) is thought to play an important role in this process in which epithelial cells shed their epithelial characteristics and acquire migratory mesenchymal cell-like properties [19]. MicroRNAs, single-stranded noncoding small (about 21 nucleotides) RNA molecules, have been shown to play a role in cellular differentiation by regulating EMT and vice versa [20,21]. Several studies have shown that culture conditions can be a potential confounding influence on the phenotype of these cells [7,18]. ARPE-19 cells cultured in Dulbecco's Modified Eagle's Medium (DMEM) with high glucose and pyruvate have recently been shown to be an excellent model to study human RPE cell function [22]. Although these cells cultured in this medium have been shown to restore pigmentation and the expression of mature RPE cell markers with western blotting, little is known about the overall gene expression profile of these cells. Therefore, we used RNA sequencing (RNA-Seq) to carry out a whole transcriptome analysis on ARPE-19 cells cultured in DMEM with high glucose and pyruvate to elucidate how the changes in gene expression might account for RPE epithelial and cellular characteristics. In this study, we observed that long-term culture induces epithelial phenotype differentiation with the dark pigmentation characteristic of RPE in ARPE-19 cells in addition to the expression of genes and proteins preferentially expressed in the RPE. In addition, miR-204 and miR-211, the two most RPE-enriched miRNAs and inducers of epithelial differentiation [8], are highly increased along with microphthalmia-associated transcription factor (MITF), the master regulator of RPE differentiation. Strikingly, RPE65 mRNA expression was greatly increased. The RNA-Seq analysis uncovered more than 3,000 differentially expressed genes. Cross-referencing with the reported transcriptome analyses of RPE cells from human embryonic stem cells, fetal tissues, and native RPE cells showed that most genes specific to RPE function are upregulated in the differentiated ARPE-19 cells. These observations suggest that the transcriptome of the differentiated ARPE-19 cells closely resembles that of the native human RPE. This study shows that ARPE-19 cells can be used to model the cellular functions of RPE, provided that low-passage cultures are appropriately cultured and differentiated.

METHODS

Cells and culture conditions: The human retinal pigment epithelial ARPE-19 cell batch used in these experiments was validated by the American Type Culture Collection (ATCC) Cell Line Authentication Service (Promega, Madison, WI) using tandem repeat analysis plus the Amelogenin gender determining locus and was a perfect match for the ATCC human cell line CRL-2302 (ARPE-19) [23]. The cells (two to three passages after authentication) were grown on Primaria® tissue culture plates in Dulbecco's modified Eagle's medium (DMEM) with 4.5 g/l glucose, L-glutamine, and 1 mM sodium pyruvate supplemented with 1% fetal bovine serum (FBS), penicillin (100 U/ml), and streptomycin (100 µg/ml; DMEM + high glucose/pyruvate/1% FBS; Thermo Fisher Scientific, Grand Island, NY), as described previously [22]. Sodium pyruvate and other media components were freshly added during the media preparation, and the prepared media were used within a week or two. The cells were maintained at 37 °C in a humidified environment of 5% CO_2 and were allowed to grow for 4 days or 4 months with media exchange performed twice a week.

Immunocytochemistry and confocal microscopy: ARPE-19 cells grown for 4 months on laminin-coated Transwell® filter inserts were blocked for 30 min with 1% bovine serum albumin (BSA) and stained for 1 h at room temperature with the following antibodies: rabbit anti-zonula occludens-1 (ZO-1, 1:200; Thermo Fisher Scientific, Waltham, MA, Cat # 61–7300), rabbit anti-claudin-2 (1:100; Thermo Fisher

Scientific, Cat # 51–6100), and mouse anti-premelanosome protein (PMEL, 1:40; Thermo Fisher Scientific, Cat # MA5–13232). Antibodies were prepared in 1% BSA supplemented with 0.1% saponin. After three 5 min washes, the cells were stained with the actin stain rhodamine-phalloidin (1:200; Cytoskeleton, Denver, CO, Cat # PHDR1) and Alexa Fluor secondary antibodies (Thermo Fisher Scientific) at 1:500 in 1% BSA for 30 min. The cells were washed three times each for 5 min, stained with 4',6-diamidino-2-phenylindole (DAPI) for 5 min, rinsed, and mounted on glass slides. Images were captured using an Andor Revolution XD spinning disk confocal microscope using the 40X Plan Fluor oil objective (NA = 1.3, WD = 0.2 mm) and the iXon x3 897 EM-CCD camera. Images were processed using Imaris x64 software (Bitplane, South Windsor, CT).

RNA-Seq library preparation and sequencing: The ARPE-19 cells cultured as described for either 4 days or 4 months were used for total RNA extraction using the miRNeasy Mini Kit (Qiagen, Valencia, CA). The RNA samples were submitted to Expression Analysis, Inc., for RNA-Seq analysis (Q^2 Solutions, Morrisville, NC). Briefly, stranded and rRNA depleted cDNA libraries were prepared from the total RNA samples using the TruSeq Stranded mRNA Sample Prep Kit (Illumina, San Diego, CA). This method preserves mRNA and other noncoding RNA species, including lncRNA, snRNA, and snoRNA. The cDNA libraries were analyzed for size distribution using an Agilent Bioanalyzer (Agilent, Santa Clara, CA) and then normalized to 2 nM in preparation using the KAPA Library Quant Kit (# KK4824, KAPA Biosystems, Wilmington, MA). The libraries were sequenced using a 2 × 50 bp paired end protocol with the median number of 87.3 million reads across all samples on the Illumina HiSeq 2500 (Illumina).

Data processing: After the sequencing was completed, the base call files were converted into FASTQ files using Illumina Software (CASAVA) and Expression Analysis developed open source programs. To prepare the reads for alignment, the sequencing adapters and other low-quality bases were clipped. The reads were aligned to External RNA Controls Consortium (ERCC) sequences to assess the success of the library construction and sequencing. A subset of the reads (about 1 million reads) were aligned to other spiked-in control sequences (PhiX and other Illumina controls used during library preparation), residual sequences (globin and rRNA), and poly-A/T sequences that persisted after clipping. The reads were also aligned to a sampling of intergenic regions to assess the level of DNA contamination. On average, about 98% of the sort-pair-end reads was mapped using the CLC genomics workbench on the GRCh38. p5 human genome release. The differential gene expression analysis (DESeq2) software package was used to identify differentially expressed transcripts [24].

Gene read counts, derived from three biologic replicates, were averaged and subjected to paired Student *t* test analysis. Expression levels were given as fragments per thousand bases of gene per million bases mapped (FPKM) for normalization. The basic statistical calculations were performed using GraphPad Prism version 6.00 for Windows (GraphPad Software, La Jolla, CA,). To identify the affected pathways and recognize shared ontological classification among differentially expressed genes, the set was examined with Gene Set Enrichment Analysis (GSEA) [25] as implemented with Pathway Studio Desktop Platform Version 9.0 (Elsevier Inc., Philadelphia, PA). The FPKM values of the RNA-Seq data from the human native RPE isolated from the nasal, temporal, and macular regions of the RPE/choroid in human eye tissue were downloaded for comparison analysis [26]. Row reads from human fetal RPE (hfRPE) and RPE derived from the H1 and H9 human embryonic stem cell (hESC) lines were downloaded from the Sequence Read Archive (SRA). Ingenuity pathway analysis (IPA) and DAVID were used for pathway analysis [27]. The data obtained were used to compare the expression levels of the genes in the RNA-Seq data set with the RNA-Seq data sets from the hESC-derived RPE and hfRPE (GSE36695), as well as the native RPE from the nasal, temporal, and macular regions of the RPE/choroid [26,28]. Scatter plots with regression lines were generated using GraphPad for each comparison. The Spearman and Pearson correlation coefficients were calculated for more than 20,000 genes.

Quantitative real-time (RT)–PCR: ARPE-19 cells cultured for either 4 days or 4 months were used for total RNA and miRNA extraction using the RNeasy Protect Mini Kit (Qiagen) and the mirVana miRNA isolation kit (Thermo Fisher Scientific), respectively. Total RNA (2 µg) was reverse transcribed using the high-capacity cDNA archive kit (Thermo Fisher Scientific). The universal cDNA synthesis kit (Exiqon, Woburn, MA) was used for cDNA synthesis from miRNA. Five microliters of cDNA was used as a template for PCR, and each PCR reaction (20 µl) was performed on the ViiA™ 7 Real-Time PCR System using various TaqMan® (Thermo Fisher Scientific) or LNA probes (Exiqon; Table 1). The manufacturer's default thermal cycling conditions were followed (40 cycles of 1 s at 95 °C and 20 s at 60 °C). *GAPDH* or *RNU1A1* were used as the reference gene for mRNA or miRNA, respectively. The results were expressed as *n*-fold induction or inhibition in gene expression relative to endogenous control calculated using the $\Delta\Delta C_T$ method.

Western blot analysis: The human RPE cells cultured for either 4 days or 4 months were washed twice with PBS (1X; 155 mM NaCl, 1.06 mM KH_2PO_4, 2.97 mM Na_2HPO_4-$7H_20$, pH 7.4, #10010-023, Gibco, Thermo Fisher Scientific), and cell extracts were prepared using cell lysis buffer according to the manufacturer's recommendation (Cell Signaling, Danvers, MA). Cell lysates containing equal amounts of protein were subjected to sodium dodecyl sulfate polyacrylamide gel electrophoresis (SDS–PAGE) using 4–12% NUPAGE Bis-Tris gels and then transferred to a nitrocellulose membrane using the iBlot® Dry Blotting System (Thermo Fisher Scientific). After blocking in 5% non-fat milk in Tris-buffered saline (TBS) containing 0.01% Tween-20 for 1 h, the membranes were incubated overnight at 4 °C with the following primary antibodies: anti-rabbit RPE65 (1:10,000, PETLET), anti-rabbit RDH5 (1:5,000, Abcam: ab101457), anti-rabbit RLBP1 (1:40,000, gift of J. Saari, University of Washington), anti-rabbit LRAT (1:5000, Abcam: ab137304), anti-mouse bestrophin (1:5,000, Abcam: ab2182), anti-mouse MERTK (1:1,000, Santa Cruz: SC-365499), anti-mouse Tyrosinase (1:1,000, Santa Cruz: SC-20035), anti-rabbit E-cadherin mAb (1:1,000, Cell Signaling: #3195), anti-mouse vimentin (1:1,000, Santa Cruz: SC-6260), and anti-rabbit ZEB1 (1:1,000, Cell Signaling: #3396). Peroxidase-conjugated goat anti-rabbit or anti-mouse immunoglobulin G (IgG) antibody was used as the secondary antibody, and the immunocomplexes were visualized with a chemiluminescence method using the enhanced chemiluminescence (ECL) Prime Western Blotting Detection Kit (GE Healthcare Life Sciences, Marlborough, MA). The blots were then stripped and reprobed with mouse monoclonal anti-α-tubulin antibody (Cell Signaling: #3873, 1:20,000).

Measurement of transepithelial electrical resistance: The membrane potential and resistance of the ARPE-19 cells in culture were measured by using the Millicell® electrical resistance system (ERS, EMD Millipore, Billerica, MA) as described previously [5,18,22]. Briefly, Transwell® (Corning, NY) polyester semipermeable filters, 0.4 µm pore size, were first coated with 5 µg/cm^2 mouse natural laminin for 6 h at

Table 1. Real-time RT–PCR primers/probes for mRNA and miRNA expression analysis.

Gene symbol	Source	Assay type	Assay ID/Catalog No.
RPE65	ThermoFisher Scientific	TaqMan	Hs01071462_m1
LRAT	ThermoFisher Scientific	TaqMan	Hs00428109_m1
RLBP1	ThermoFisher Scientific	TaqMan	Hs00165632_m1
RDH5	ThermoFisher Scientific	TaqMan	Hs01123934_g1
RDH10	ThermoFisher Scientific	TaqMan	Hs00416907_m1
BEST1	ThermoFisher Scientific	TaqMan	Hs00188249_m1
TYR	ThermoFisher Scientific	TaqMan	Hs00165976_m1
MERTK	ThermoFisher Scientific	TaqMan	Hs01031973_m1
KL	ThermoFisher Scientific	TaqMan	Hs00183100_m1
TYRO3	ThermoFisher Scientific	TaqMan	Hs00170723_m1
AXL	ThermoFisher Scientific	TaqMan	Hs01064444_m1
CDHI	ThermoFisher Scientific	TaqMan	Hs01023894_m1
CDH2	ThermoFisher Scientific	TaqMan	Hs00983056_m1
CDH3	ThermoFisher Scientific	TaqMan	Hs00999915_m1
TJP1	ThermoFisher Scientific	TaqMan	Hd01551861_m1
VIM	ThermoFisher Scientific	TaqMan	Hs00958111_m1
CCDN1	ThermoFisher Scientific	TaqMan	Hs00765553_m1
MITF	ThermoFisher Scientific	TaqMan	Hs01117294_m1
TRPM1	ThermoFisher Scientific	TaqMan	Hs00931865_m1
TRPM3	ThermoFisher Scientific	TaqMan	Hs00257553_m1
GAPDH	ThermoFisher Scientific	TaqMan	Hs99999905_m1
miR-204-5p	Exiqon	SYBR Green	# 206072
miR-211-5p	Exiqon	SYBR-Green	# 204009
RNUIA1	Exiqon	SYBR-Green	# 308015

room temperature and washed once with PBS. The ARPE-19 cells were plated on 12-well, 12 mm diameter Transwell® inserts at a density of 300,000 cells/cm^2 and were allowed to grow for 4 months with media exchange performed twice a week. Transepithelial electrical resistance (TER) was measured using STX3 chopstick electrodes, and the net TER values ($\Omega \times cm^2$) were calculated by subtracting the value of blank from the value recorded for each individual filters plated with cells and multiplying the background subtracted TER values by the area of the Transwell® filter membranes. A minimum of six independent Transwell® filters were used in each experimental condition and repeated in two separate experiments.

Retinoid analysis: All procedures involving retinoids were conducted under dim red light. ARPE-19 cells were grown on Transwell® polyester semipermeable filters (Corning, NY), 0.4 µm pore size, for 4 months in DMEM + high glucose/pyruvate/1% FBS medium. The cells were then washed twice with serum-free media, treated with or without 4 µM all-*trans* retinol given basally (the outer chamber) in serum-free media and then incubated overnight in a humidified environment of 5% CO_2 at 37 °C. Serum-free media from the apical (inner) chamber were collected, and the retinoids were extracted in the presence of hydroxylamine. Briefly, serum-free media were mixed with 1 ml of freshly made hydroxylamine buffer (50 mM MOPS, 10 mM NH_2OH, pH 6.5) and with 1 ml ethanol and then incubated in the dark for 30 min at room temperature. Following this, the retinoids were extracted twice with the addition of 4 ml hexane, vortexing, and centrifugation (2,000 ×*g*, 8 min). The upper hexane phases were collected and pooled, and solvent was evaporated under a gentle stream of argon. The dried samples were dissolved in 50 µl hexane and then analyzed with high-performance liquid chromatography (HPLC). In addition, the cells were washed, harvested, and then homogenized in PBS (pH 7.4) using a disposable microtissue homogenizer (BioMasher II, Warrington, PA). The cell homogenates were extracted into hexane (as above). Retinaloxime standards were prepared following the protocol of Garwin and Saari [29]. Briefly, 0.5 µmol authentic all-*trans*-retinal (Sigma-Aldrich Corp., St. Louis, MO), or 11-*cis*-retinal (Toronto Research Chemicals, Toronto, Canada), dissolved in 1 ml ethanol was incubated in the presence of 10 mM hydroxylamine, 10 mM MOPS, pH 6.5, for 30 min in the dark at room temperature. The newly formed retinaloximes were extracted twice with the addition of 4 ml hexane. The upper hexane phases were combined and solvent was evaporated under a gentle stream of argon. Standards and samples were separated on a LiChrospher Si-60 (5 µm; ES Industries, West Berlin, NJ) normal-phase column using a 4.5% ethyl acetate, 0.5% dioxane (v/v) in the hexane mobile phase at a flow rate of 1.2 ml/min. Absorbance was monitored at 365 and 325 nm for the presence of retinaloxime and retinylester, respectively. Data were analyzed using Empower 3 software (Waters Corp., Milford, MA).

STRING interaction analyses: Potential interactions among selected genes were analyzed using Search Tool for the Retrieval of Interacting Genes/Proteins (STRING), a database and web resource dedicated to protein–protein interactions, including physical and functional interactions [30]. The gene IDs of the up- and downregulated genes were used as an input in the online database to find the associations derived from several computational predicted and experimentally determined functional associations and protein–protein interactions. The result was graphically displayed with different colored edges indicating the type of evidence.

Statistical analysis: All values are expressed as mean ± standard deviation (SD), n = 4. For statistical significance, the paired Student *t* test in Excel was used. A p-value of less than 0.05 denotes statistically significant differences. The results shown are representative of three or more independent experiments.

RESULTS

ARPE-19 cells exhibit RPE characteristics after prolonged culture: Maintenance of native RPE characteristics by ARPE-19 cells depends on how they are cultured and passaged. In addition, these cells undergo dedifferentiation during culture, and this particular phenomenon appears to be a product of cell substrate and growth media [18,22,31]. Figure 1 illustrates the typical growth of the ARPE-19 cells cultured on 100 mm Primaria® Petri dishes. Initially, the ARPE-19 cells cultured in DMEM with 4.5 g glucose and 1 mM sodium pyruvate and supplemented with 1% FBS (DMEM + high glucose/pyruvate/1% FBS) show non-epithelial morphology while they are subconfluent and mitotically active (Figure 1A). They attain morphology reminiscent of fibroblasts after 4 days of reaching confluence (Figure 1B) and remain in elongated fibroblastic morphology for more than 2 weeks under these culture conditions. However, the cells grown in culture for 1 month exhibit islands of hexagonally packed epithelial-like cells characteristic of the RPE (Figure 1C). As the cell cultures mature, they increasingly exhibit characteristics of the RPE, such as well-defined cell borders and an increase in pigmentation (indicative of de novo synthesis of melanin pigment). This differentiation required 3–4 months after cultures reach a confluent density. The long-term cultures developed features characteristic of the native RPE, including the typical cobblestone epithelial morphology and heavy pigmentation often visible to the naked eye (Figure

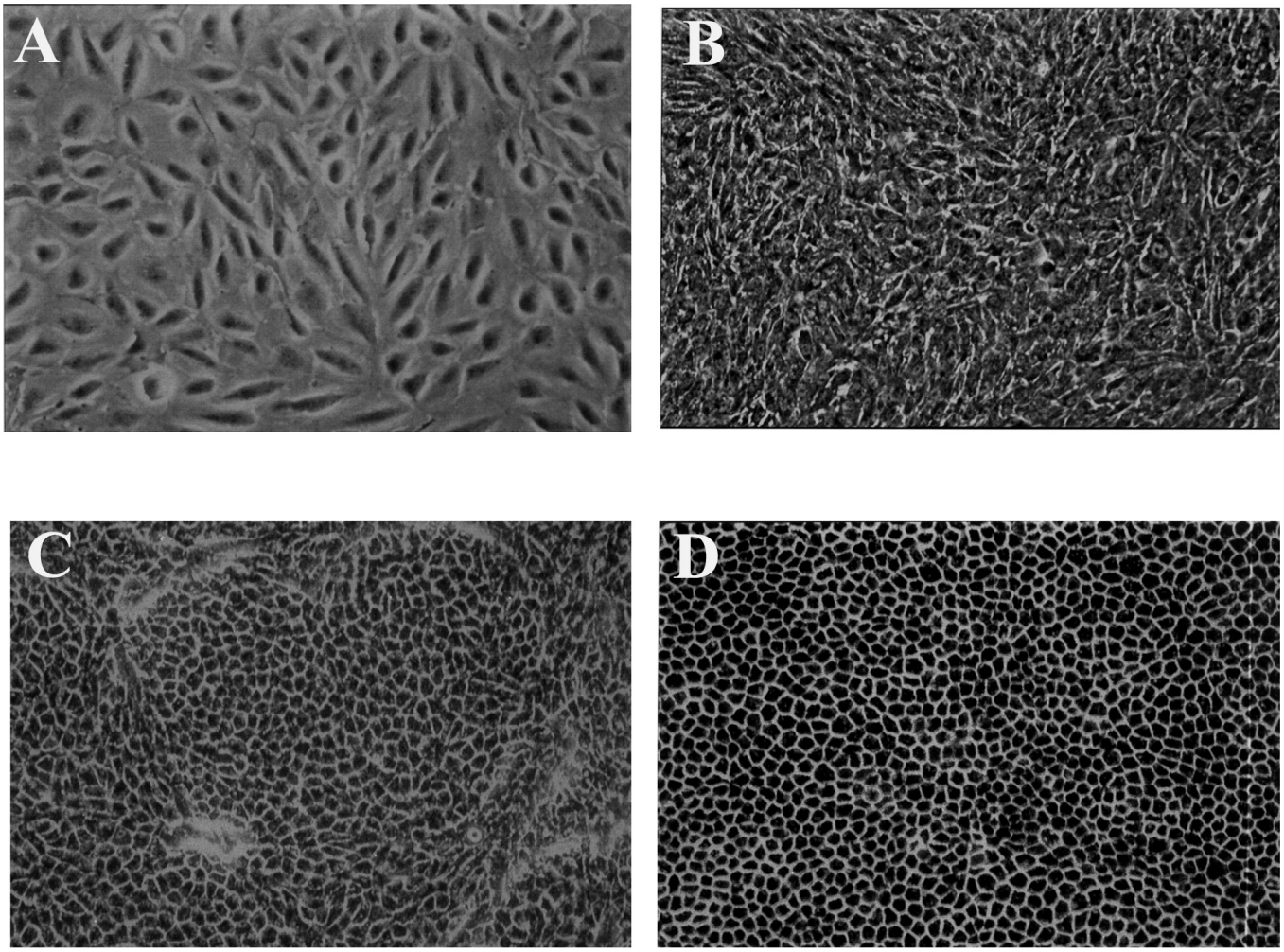

Figure 1. ARPE-19 cells develop RPE phenotype characteristics during differentiation. ARPE-19 cells were grown for various time periods as outlined in the Methods section, and the morphology of the cells was examined with phase-contrast microscopy. **A**: Subconfluent cells 1 day after plating. **B**: Cells grown for 4 days. **C**: Cells grown for 4 weeks. **D**: Cells grown for 4 months. Magnification, 100X.

1D), an important structural feature characteristic of native RPE cells. These cells remain well differentiated and form a monolayer of pigmented cells resembling differentiated RPE cells in vivo even after a year in culture (data not shown).

To characterize further the phenotypic changes associated with differentiation, we examined the existence of tight junctions (Figure 2B) between adjacent cells, an important structural feature of native RPE monolayers [32], in the ARPE-19 cells cultured for 4 months. We examined the expression and localization of the tight junction-associated protein ZO-1, claudin-2, and actin with immunocytochemistry and confocal microscopy. These cells express the tight junction complex protein ZO-1, predominantly localized to the cell edges within the cultured RPE cells, suggesting that these differentiated RPE culture form continuous cell–cell contact with tight junctions. Claudin-2 expression was also localized to the tight junction complex uniformly across the monolayer in the differentiated RPE cells (Figure 2D,E) and was detected along with ZO-1 in the junctional complex (Figure 2F, merged). In addition, the actin cytoskeleton in these cells is distributed at the cell periphery along the tight junctions, closely resembling that of the native RPE (Figure 2C). We also observed the expression of PMEL (also known as PMEL17), an integral membrane protein exclusively expressed in pigmented cells, in the differentiated ARPE-19 cells (Figure 2A). In addition, we used the Millicell® electrical resistance system to measure the TER, a common methodology for measuring the barrier function that is often taken as an indicator of the permeability and resistance of tight junctions [33]. ARPE-19 cells plated on laminin-coated Transwell® filters were grown in DMEM + high glucose/pyruvate/1% FBS for the duration of the experiment. The

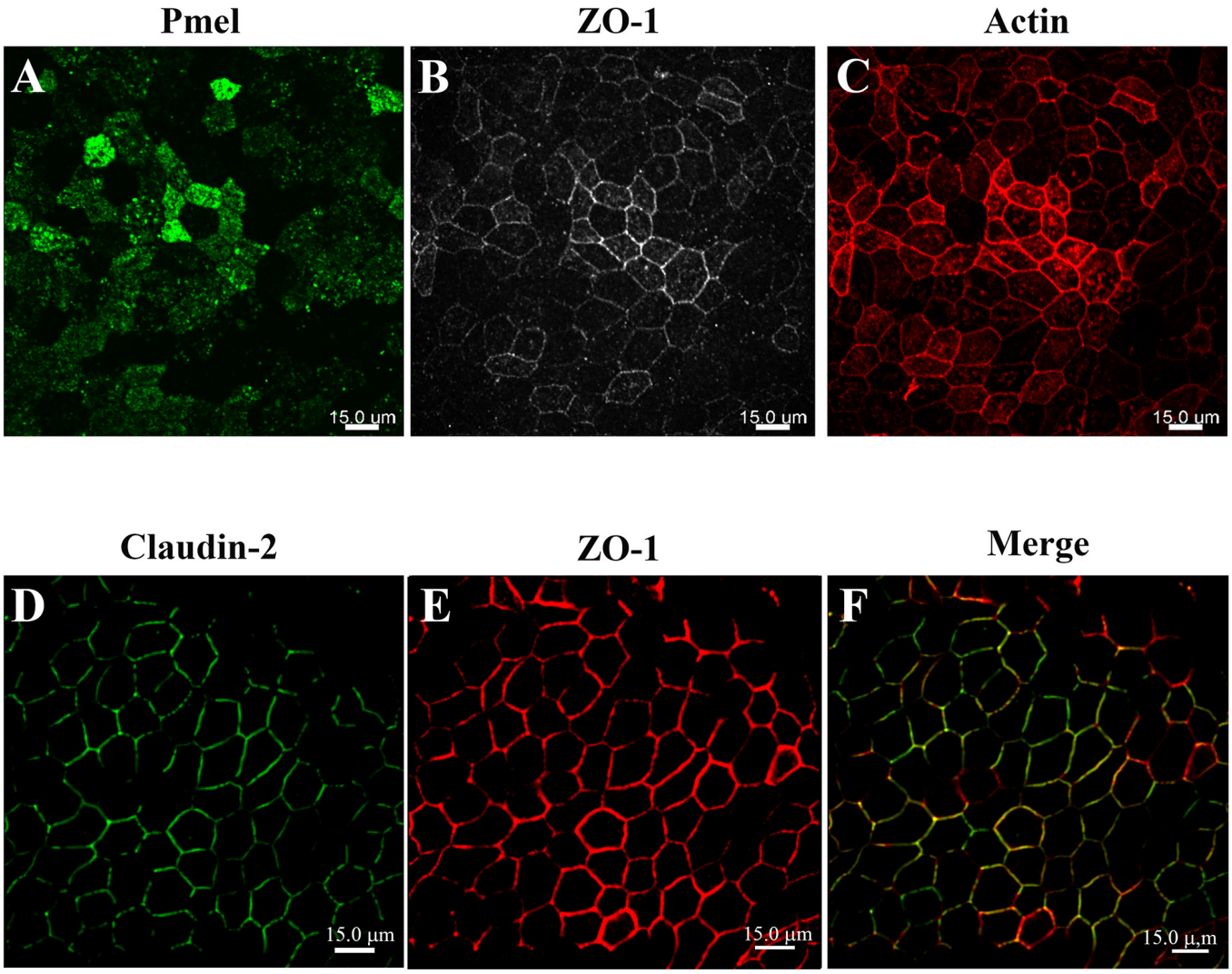

Figure 2. Confocal micrographs of ARPE-19 cells cultured for 4 months. The ARPE-19 cells were plated on laminin-coated Transwell® filter membrane at a density of 3×10^5 cells/cm^2 and grown for 4 months as outlined in the Methods section. Rabbit anti- zonula occludens-1 (ZO-1), mouse anti-premelanosome protein (PMEL), mouse anti-claudin-2 primary antibodies, and Alexa Fluor secondary antibodies were used to immunostain the ARPE-19 cells at 4 months post-confluency; rhodamine-phalloidin was used to stain actin. **A**: PMEL immunostaining correlates with the presence of melanosome pigmentation. **B**: ZO-1 immunostaining shows good junctional development and localization at the cell borders containing a mixture of elongated and polygonal cells. **C**: Actin immunostaining reveals circumferential actin distribution throughout the height of the cells. **D**: Claudin-2 immunostaining shows tight junction localization uniformly across the monolayer. **E**: ZO-1 immunostaining shows good junctional development and localization at the cell borders regardless of the secondary antibody used. **F**: Claudin-2 immunofluorescent labeling shows colocalization with ZO-1 in the tight junction complexes (merged image of **D** and **E**). Images were taken using an Andor Revolution XD spinning disk confocal microscope using the 40X Plan Fluor oil immersion objective. Scale bar = 15 µm.

barrier properties of the culture were measured via TER, and a mean level of 126 ± 26 Ω × cm^2 TER (n = 12) was observed in the cells cultured for 4 months.

Differentiation-induced changes in gene expression: To determine whether changes in gene expression might account for acquisition of the RPE phenotype, we performed a whole transcriptome RNA-Seq analysis of the RPE cells kept in culture for 4 days and for 4 months. The ARPE-19 cells were seeded at low density, and cells were collected at 4 days while subconfluent or at 4 months when they had acquired the typical cobblestone epithelial morphology with heavy pigmentation. RNA-Seq yielded approximately 84.1 million on-target reads from the median number of 87.3 million actual reads for each of the six cDNA libraries (three from the cells cultured for 4 days and three from the cells cultured

for 4 months) obtained from the pooled cultured cells. The reads were aligned to the human genome issue hg38 using the CLC genomics workbench. The differential gene expression analysis (DESeq2) software package was used to identify differentially expressed transcripts [24]. Detailed RNA-Seq data associated with this publication are available through the Gene Expression Omnibus (GEO; GSE88848). Overall, an average of 98% of the reads aligned to the transcriptome. The gene compilation for this particular analysis consists of 27,939 genes and 77,612 isoforms. Volcano plots were used to visualize the differential gene expression between the RPE cells cultured for 4 days and for 4 months and the distribution of the fold changes and the p-values of the 27,939 genes (Figure 3). To identify genes that are differentially expressed, a fold-change criterion was employed with the mean fold change between 4 months versus 4 days to be ≥2.5 or ≤-2.5. Of the 16,736 genes with detectable signals, about 1,681 (9.96%) genes were upregulated, and approximately 1,629 (9.72%) genes were downregulated with a fold change of 2.5 or more differences between 4 months and 4 days. The genes were then ranked by their greatest fold change to better characterize differentially expressed genes with critical functions within the RPE.

Table 2 comprises the genes most highly upregulated in the differentiated RPE cells cultured for 4 months, genes previously identified as RPE marker genes, or genes with functions characteristic of differentiated RPE cells [34-38]. The database is based upon Gene Ontology and scientific literature curated by Pathway Studio/Elsevier. Gene Ontology analysis showed that these upregulated genes are associated with, for example, visual cycle, phagocytosis, pigment synthesis, cell differentiation, and RPE-related transcription factors. Among the most highly upregulated genes, ranked by fold change, are the pigmentation-related genes, *DCT* (OMIM 191275), *TRPM1* (OMIM 603576), *OCA2* (OMIM 611409), *TYRP1* (OMIM 115501), and *TYR* (OMIM 606933). The gene with the largest increase (2,840 fold) was *DCT*, an important regulatory enzyme that plays a pivotal role in the biosynthesis of melanin [39]. All the genes associated with the visual cycle, *RPE65* (OMIM 180069), *LRAT* (OMIM 604863), *RLBP1* (OMIM 180090), *RDH5* (OMIM 601617), *RBP1* (OMIM 180260), and *RDH10* (OMIM 607599), were also highly increased. In particular, *RPE65* had a more than 1,460-fold increase in gene expression in the differentiated RPE cells cultured for 4 months. Genes that have been reported to be associated with phagocytosis were also highly increased in the RPE cells cultured for 4 months. In particular, the expression of *MERTK* (OMIM 604705), an indispensable receptor for POS internalization [40], and *ITGAV* (OMIM 193210; integrin αv), which promotes POS recognition and binding [41], were increased by 17- and 12-fold, respectively.

Genes whose expression correlates with the state of confluence, and are preferentially expressed in differentiated cells, were highly increased in the RPE cells cultured for 4 months. In particular, the expression of death associated protein-like 1 (*DAPL1; Gene ID: 92196*), abundantly expressed in the retina/RPE transcriptome and involved in early stages of epithelial differentiation [42], was increased by more than 1,900-fold in the differentiated RPE cells. Genes known to be abundantly expressed in the RPE, and that play a protective role in RPE function, such as *PEDF* (OMIM 172860; 190-fold) and cystatin C (*CST3*, OMIM 604312; 44-fold), were also highly increased. The expression of claudin 2 (*CLDN2;* OMIM 300520), which plays an important role in determining tight junction selectivity and permeability, was significantly upregulated (210-fold) in the differentiated ARPE-19 cells. In addition, with the RT–PCR analysis, we confirmed that the expression of claudin 3 (OMIM 602910; *CLDN3*, ΔCT = 29) and claudin 19 (OMIM 610036; *CLDN19,* ΔCT = 35), the major claudin of human RPE, were slightly increased in the differentiated ARPE-19 cells, supporting the RNA-Seq observations (data not shown). However, the level of expression of *claudin 3* and *claudin 19* was lower than that of *claudin 2* (ΔCT = 26). E-cadherin (*CDH1*; OMIM 602910) and P-cadherin (*CDH3*; OMIM 114021), epithelial markers expressed in the native RPE monolayer, were highly increased compared to the RPE cells in culture for 4 days. Several RPE-associated transcription factors, such as PAX6 (which synergizes with MITF to activate the expression of genes involved in pigment biogenesis [43]), SOX9 (a key regulator of visual cycle genes [44]), OTX2 (which regulates RPE specification during retina development [45]), and MITF [46,47], were all observed to be significantly upregulated in the differentiated ARPE-19 cells cultured for 4 months that resembled the native RPE phenotype.

Table 3 shows selected genes that were downregulated with a mean fold change of ≤ 2.0 in the differentiated ARPE-19 cells that were cultured for 4 months. The majority of the most down- regulated genes play a role in the cell cycle and its regulation, based on the Gene Ontology analysis. For example, in the RPE cells cultured for 4 months, the expression of transforming growth factor beta 1 (*TGFβ1*; OMIM 190180), a major inducer of EMT [48], decreased by more than 21-fold compared to the cells that were cultured for 4 days. In addition, the expression of cyclin-dependent kinase 1 (*CDK1*; OMIM 116940), an important factor in determining the cell cycle timing of mitosis by interacting with cyclin

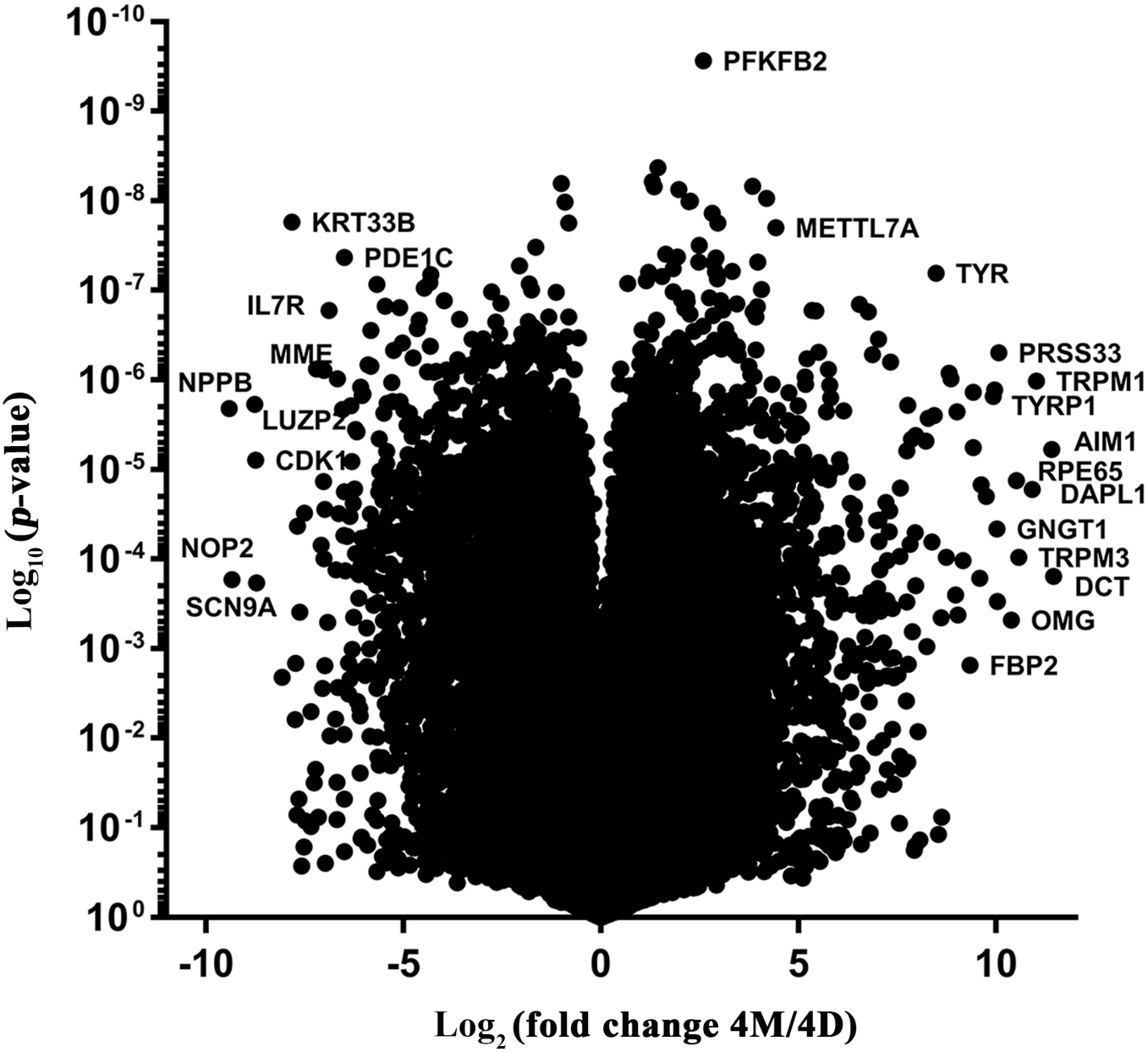

Figure 3. Volcano plot showing differentially expressed genes in the differentiated RPE cells. ARPE-19 cells grown for either 4 days or 4 months in DMEM were used for total RNA extractions and were used for RNA-Seq analysis, as described in the Methods section. Volcano plot for the 27,939 genes of the RPE cells cultured for 4 days and for 4 months. Representative highly up- or downregulated genes at high statistical significance are labeled.

B, decreased by more than 31-fold in the differentiated RPE cells.

RPE differentiation promotes expression of RPE-specific visual cycle genes and proteins: The expression of key enzymes of the visual cycle is widely used as a marker for RPE-specific differentiation. We examined the expression of visual cycle genes in the ARPE-19 cells cultured for 4 days or 4 months with RT–PCR (Figure 4A). All genes associated with the visual cycle (*RPE65*, *CRALBP*, *LRAT*, *RDH5*, and *RDH10*) showed increased expression in the differentiated ARPE-19 cells cultured for 4 months, supporting the RNA-Seq observations. In particular, the mRNA expression of *RPE65* was increased more than 10,000-fold in the ARPE-19 cells cultured for 4 months compared with the cells cultured for 4 days.

Table 2. Selected upregulated genes in the differentiated RPE cells.

Gene	Gene Name	Biological Function	p-value	4 Days	4 Months	FC 4M/4D
Vitamin A Metabolism						
RPE65	Retinal Pigment Epithelium-Specific Protein 65kDa	Visual pigment regeneration	1.32E-05	0.01	9.75	1462.50
TTR	Transthyretin	Retinol transport	1.04E-05	0.00	3.98	1326.67
RGR	Retinal G Protein Coupled Receptor	Receptor for retinal	5.43E-04	0.02	15.98	959.00
RLBP1	Retinaldehyde Binding Protein 1	Retinol regeneration	2.50E-04	0.39	198.37	504.32
BCMO1	Beta-Carotene 15,15-Monooxygenase 1	Beta-carotene metabolism	8.39E-06	0.13	35.68	281.66
RDH5	Retinol Dehydrogenase 5	Retinal biosynthesis	2.76E-04	4.02	100.39	24.95
LRAT	Lecithin Retinol Acyltransferase	Esterification of all-trans-retinol	6.55E-04	0.41	9.13	22.44
RBP1	Retinol Binding Protein 1,	Cellular Retinol transport	1.37E-04	12.32	37.44	3.04
STRA6	Stimulated by Retinoic Acid 6	Retinol transport	1.38E-02	0.12	0.25	2.14
RDH10	Retinol Dehydrogenase 10	Retinal biosynthesis	1.65E-05	90.34	181.83	2.01
Phagocytosis						
COLEC12	Collectin Sub-Family Member 12	Phagocytosis	2.32E-05	0.64	94.98	148.40
PLA2G5	Phospholipase A2, Group V	Phagocytosis	1.42E-07	0.12	10.88	93.29
TUB	Tubby Bipartite Transcription Factor	Phagocytosis	5.67E-06	0.01	0.45	67.00
MERTK	MER Proto-Oncogene, Tyrosine Kinase	Phagocytosis	1.73E-05	0.42	7.00	16.81
ITGAV	Integrin, Alpha V	Signal transduction	5.63E-04	3.08	35.91	11.65
Pigmentation						
DCT	Dopachrome Tautomerase	Melanin synthesis	1.50E-04	0.02	47.34	2840.20
TRPM1	Transient Receptor Potential Cation Channel, M1	Melanin synthesis	4.01E-06	0.01	36.23	2717.26
OCA2	Melanocyte-Specific Transporter Protein	Melanosome maturation	1.01E-03	0.00	4.06	1352.22
TYRP1	Tyrosinase-Related Protein 1	Melanin biosynthesis	1.28E-06	3.77	3749.82	995.53
TRPM3	Transient Receptor Potential Cation Channel, M3	Calcium signaling	6.89E-05	1.50	647.81	432.84
TYR	Tyrosinase	Melanin biosynthesis	6.43E-08	0.77	273.39	356.60
PMEL	Premelanosome Protein	Biogenesis of melanosomes	6.45E-05	1.27	136.65	107.60
SLC45A2	Solute Carrier Family 45, Member 2	Melanin biosynthesis	1.04E-04	1.42	69.92	49.12
Cell Differentiation						
DAPL1	Death Associated Protein-Like 1	Epithelial cell differentiation	1.67E-05	0.34	663.95	1933.85
CP	Ceruloplasmin (Ferroxidase)	Iron metabolism	2.33E-04	0.51	136.22	265.36
DSC1	Desmocollin 1	Cell adhesion	4.30E-06	0.12	30.33	245.92
CLDN2	Claudin 2	Tight junction	2.06E-03	0.02	3.51	210.8
SERPINF1	PEDF	Anti-angiogenesis	1.61E-05	7.76	1478.63	190.46
FGFR2	fibroblast growth factor R2	Cell cycle	2.28E-05	0.12	17.51	142.00

Molecular Vision 2017; 23:60-89 <http://www.molvis.org/molvis/v23/60>

Gene	Gene Name	Biological Function	p-value	4 Days	4 Months	FC 4M/4D
BEST1	Bestrophin 1	Electron transport	3.41E-04	0.30	13.06	44.01
CST3	Cystatin c	Protease inhibitor	1.35E-04	66.06	2013.58	30.48
CDH3	Cadherin 3, P-Cadherin	Cell adhesion	1.44E-03	0.02	0.50	24.83
CDH1	Cadherin E	Cell adhesion	8.79E-05	0.04	0.57	13.23
RPE-related Transcription Factor						
TFEC	Transcription Factor	Transcriptional regulation	1.91E-07	0.08	4.63	57.88
SOX9	SRY -Box 9	Transcriptional regulation	1.21E-03	4.90	21.77	4.44
OTX2	Orthodenticle Homeobox 2	Sensory organ development.	8.13E-07	38.35	150.33	3.92
MITF	Microphthalmia-Associated	Melanocyte development	1.21E-07	50.91	119.18	2.34
CRX	Cone-Rod Homeobox	Transcriptional regulation	8.82E-03	1.07	1.33	1.25
PAX6	Paired Box 6	Eye development	1.79E-02	28.42	33.87	1.19

Transcript fold change and adjusted p-value of transcripts between 4 days and 4 months cultured RPE cells, and were considered significantly changed with adjusted $p<0.05$ and fold change of at least 2.0

Molecular Vision 2017; 23:60-89 <http://www.molvis.org/molvis/v23/60>

Table 3. Selected downregulated genes in the differentiated RPE cells.

Gene	Gene Name	Biological Function	p-value	4 Days	4 Months	FC 4M/4D
Cell Cycle						
TGFBI	Transforming Growth Factor	Cell cycle	2.01E-06	417.62	19.64	0.047
SERPINE1	Serpin Peptidase	Inhibitor of fibrinolysis	1.48E-05	255.38	13.21	0.052
TAGLN	Transgelin	Cell cycle	3.11E-06	181.82	8.52	0.047
NPPB	Natriuretic Peptide B	Cell proliferation	2.07E-06	162.61	0.24	0.001
CDK1	Cyclin-Dependent Kinase 1	Cell cycle	6.96E-05	37.73	1.22	0.033
CPA4	Carboxypeptidase A4	Proliferation	6.31E-07	37.03	1.39	0.038
UBE2C	Ubiquitin-Conjugating Enzyme	Cell cycle	1.03E-06	20.57	0.17	0.008
CENPF	Centromere Protein F	Cell cycle	4.56E-04	20.27	1.98	0.098
CEP55	Centrosomal Protein 55 kDa	Cell cycle	1.21E-05	18.57	0.31	0.017
CDC6	Cell Division Cycle 6	Cell cycle	2.06E-05	15.16	0.72	0.047
CCNB2	Cyclin B2	Cell cycle	1.41E-05	12.76	0.45	0.036
BUB1	BUB1 Serine/Threonine Kinase	Cell cycle	4.44E-06	10.99	0.58	0.053
BIRC5	Baculoviral IAP Repeat	Cell cycle	2.84E-05	10.17	0.13	0.013
CCNE2	Cyclin E2	Cell cycle	3.27E-05	9.71	0.46	0.047
CDC20	Cell Division Cycle 20	Cell cycle	9.49E-06	8.60	0.24	0.028
MKI67	Marker of Proliferation K-67	Cell proliferation	2.19E-04	5.45	0.16	0.029
AURKB	Aurora Kinase B	Cell Cycle	5.15E-08	5.12	0.13	0.025
E2F1	E2F Transcription Factor 1	Cell cycle	1.29E-07	4.38	0.28	0.064
PLK1	Polo-Like Kinase 1	Cell cycle	5.67E-05	2.91	0.12	0.041
CDC25C	Cell Division Cycle 25C	Cell cycle	1.71E-04	2.31	0.08	0.033
Transcription Factors						
ANKRD1	Ankyrin Repeat Domain 1	Transcription	1.49E-07	326.21	7.39	0.023
HIST2H3C	Histone Cluster 2 H3c	Transcription	6.75E-07	66.71	1.12	0.017
TOP2A	Topoisomerase (DNA) II Alpha	Transcription	6.18E-05	37.41	0.74	0.020
PTTG1	Pituitary Tumor-Transforming 1	Transcription	1.99E-05	31.15	1.78	0.057
JUN	Jun Proto-Oncogene	Transcription	4.00E-05	29.84	2.79	0.093
RRM2	Ribonucleotide Reductase M2	Transcription	1.06E-05	14.39	0.71	0.049

Transcript fold change and adjusted p-value of transcripts between 4 days and 4 months cultured RPE cells, and were considered significantly changed with adjusted $p<0.05$ and fold change of at least 2.0.

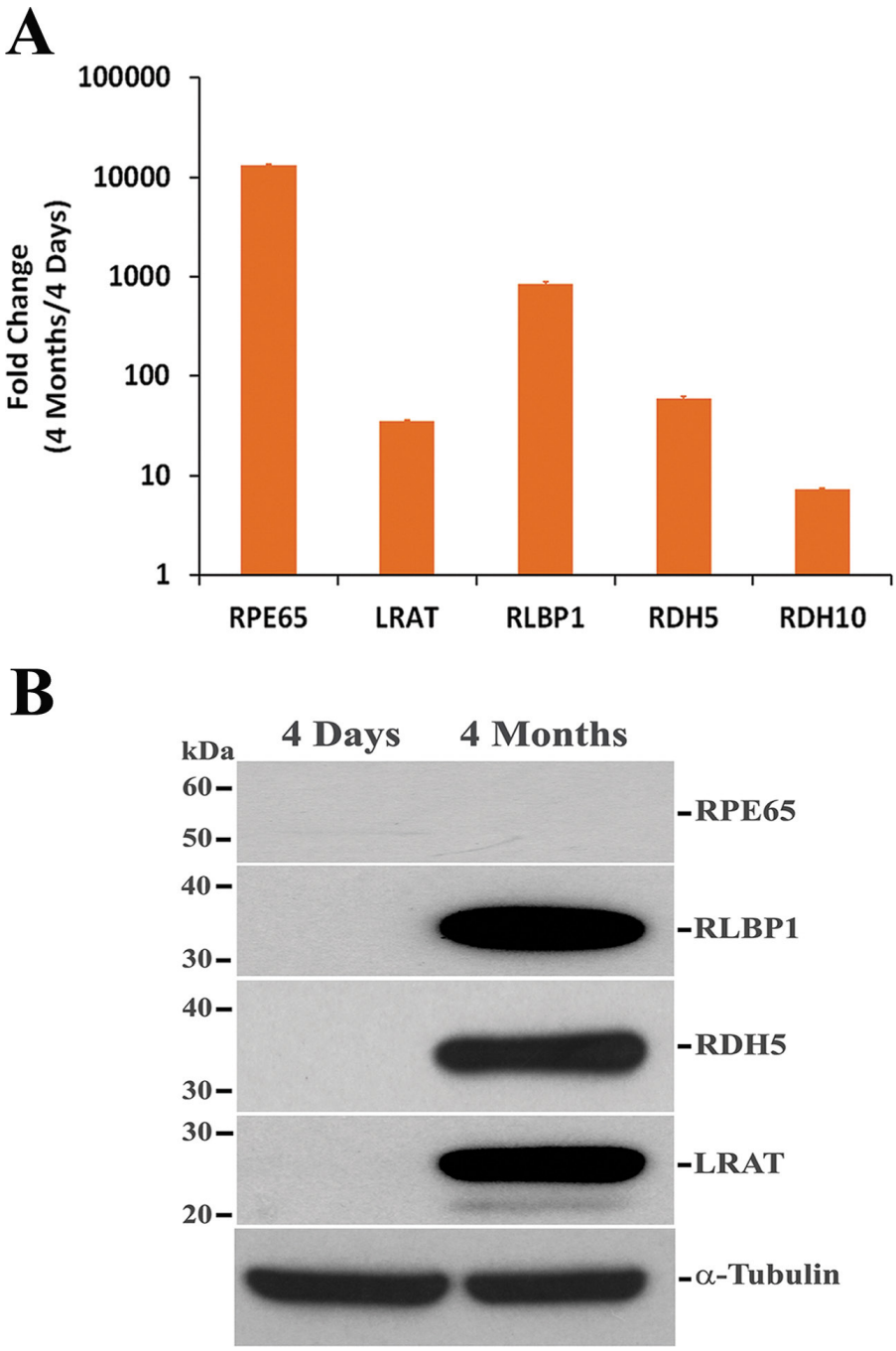

Figure 4. Expression of visual cycle genes increases in the differentiated RPE cells. ARPE-19 cells grown for either 4 days or 4 months were used for total RNA and protein extractions and were used for real-time quantitative PCR and western blotting, respectively, as described in the Methods section. **A**: Real-time PCR analysis of RPE-specific mRNA expression. The values are mean ± standard deviation (SD), n = 4. *p<0.001 compared with control. **B**: Western blot analysis of the expression of the RPE-specific proteins. α-Tubulin expression shows that the amount of protein used in the different samples is similar.

To assess the effect of these increases in the mRNA expression of the visual cycle genes on their respective protein expression in the differentiated cells, we performed western blot analysis. Immunoreactive bands specific for CRALBP, RDH5, and LRAT were detected only in the cells cultured for 4 months and not in the RPE cells cultured for 4 days (Figure 4B). The observed increases in the expression of the visual cycle protein correlated well with the increase in mRNA expression. However, expression of the RPE65 protein was undetectable on immunoblots in the differentiated and un-differentiated RPE cells (Figure 4B).

Retinoid analysis: As we observed the expression of proteins, except RPE65, that are essential for the retinoid visual cycle in the differentiated ARPE-19 cells cultured for 4 months, we examined whether the RPE cells grown for 4 months in Transwell® inserts were able to take up all-*trans* retinol and convert it to all-*trans* retinyl esters. To observe the ester formation, ARPE-19 cells grown for 4 months in the Transwell® inserts were incubated with or without 4 µM all-*trans* retinol added into the basal chamber, and the plates were incubated at 37 °C for 16 h in the dark. Following extraction, the retinoids in the ARPE-19 cells were analyzed with HPLC and monitored at 325 nm. As shown in Figure 5A, the formation of retinyl esters was evident with detectable amounts of all-*trans* retinyl esters in treated cells. The observed formation of the all-*trans* retinyl esters was corroborated by the observed chromatogram of authentic all-*trans* retinyl palmitate standard and its corresponding absorbance spectrum (Figure 5B). No traceable all-*trans* retinyl ester peak was observed in the untreated control cells.

RPE differentiation increases the expression of melanogenesis and phagocytosis genes and proteins: We examined several RPE-specific genes expressed in native RPE cells. As seen in Figure 6A, bestrophin-1 (*BEST1*; OMIM 607854), a calcium-sensitive chloride channel predominantly expressed in the basolateral membrane of the RPE [49], was highly increased (about 100-fold) in the differentiated ARPE-19 cells. Tyrosinase (*TYR*), a rate-limiting enzyme responsible for melanin biosynthesis in the RPE [50], was increased close to 10,000-fold, and the expression of the klotho (*KL*; OMIM 604824) gene, a regulator of melanin biosynthesis [51], was also increased greatly, indicating that these cells are able to produce the melanin pigment under these culture conditions, consistent with the observed dark pigmentation. In addition, expression of MER tyrosine kinase (*MERTK*), a receptor found at the apical surface of the RPE that plays a critical role in phagocytosis of shed ROS [52], was increased by more than 15-fold in the differentiated RPE cells. However, the expression of *TYRO3* (OMIM 600341) and *AXL* (OMIM 109135), fellow TAM family members with *MERTK*, was downregulated in the cells cultured for 4 months.

Western blot analysis was performed to corroborate the RNA results (Figure 6B). Corresponding to the mRNA expression, the bestrophin-1 protein was increased in the differentiated RPE cells. Similarly, the tyrosinase and MERTK proteins were detected in the cells cultured for 4 months and not in the cells cultured for 4 days.

Differentiated RPE cells exhibit epithelial specific gene expression: To further characterize the phenotypic changes associated with differentiation, we examined the expression of established markers typical for nonepithelial and epithelial cells. We found that mRNA expression of E-cadherin (*CDH1*), an epithelial morphoregulatory protein [53], was highly increased in the ARPE-19 cells cultured for 4 months (Figure 7A) as was E-cadherin protein expression (Figure 7B). Similarly, the mRNA expression of P-cadherin (*CDH3*), an epithelial cadherin coexpressed with E-cadherin [53], was also highly increased (Figure 7A). However, the expression of N-cadherin (*CDH2*; OMIM 114020), which is typically found in nonepithelial cells [53], was decreased in the cells cultured for 4 months. In addition, the expression of another widely used nonepithelial marker vimentin [54] was also decreased. The vimentin (*VIM*; OMIM 193060) mRNA and protein were highly expressed in the cells cultured for 4 days, and the expression decreased in the differentiated cells cultured for 4 months (Figure 7A,B). Interestingly, in addition to the predicted 57 kDa protein band for vimentin, we noticed two additional bands of lower intensity and lower molecular weight in the cells cultured for 4 months.

An important structural feature that cultured RPE cells should retain is the barrier function performed by tight junctions. ZO-1 is an important regulator of tight junctions [19]. Here, we observed that the expression of *TJP1* (OMIM 601009; Figure 7A), the gene that codes the tight junction protein ZO-1, was significantly increased in the cells cultured for 4 months. The higher level of *TJP1* would correlate with the acquired epithelial morphology characteristic of the native quiescent RPE cells. Expression of cyclin D1 (*CCND1*; OMIM 168461), an activator of cell cycle progression, which regulates progression of cells from the G1 to S phase [55], was decreased in the RPE cells cultured for 4 months compared with the cells cultured for 4 days (Figure 7A).

Differentiation increases the expression of miR-204 and miR-211: MiR-204 and -211, the two most highly expressed miRNAs in primary cultures of human fetal RPE, play a critical role in RPE epithelial barrier function and differentiation [8,56]. Therefore, we examined miR-204 and miR-211 expression in the differentiated RPE cells with RT–PCR. As

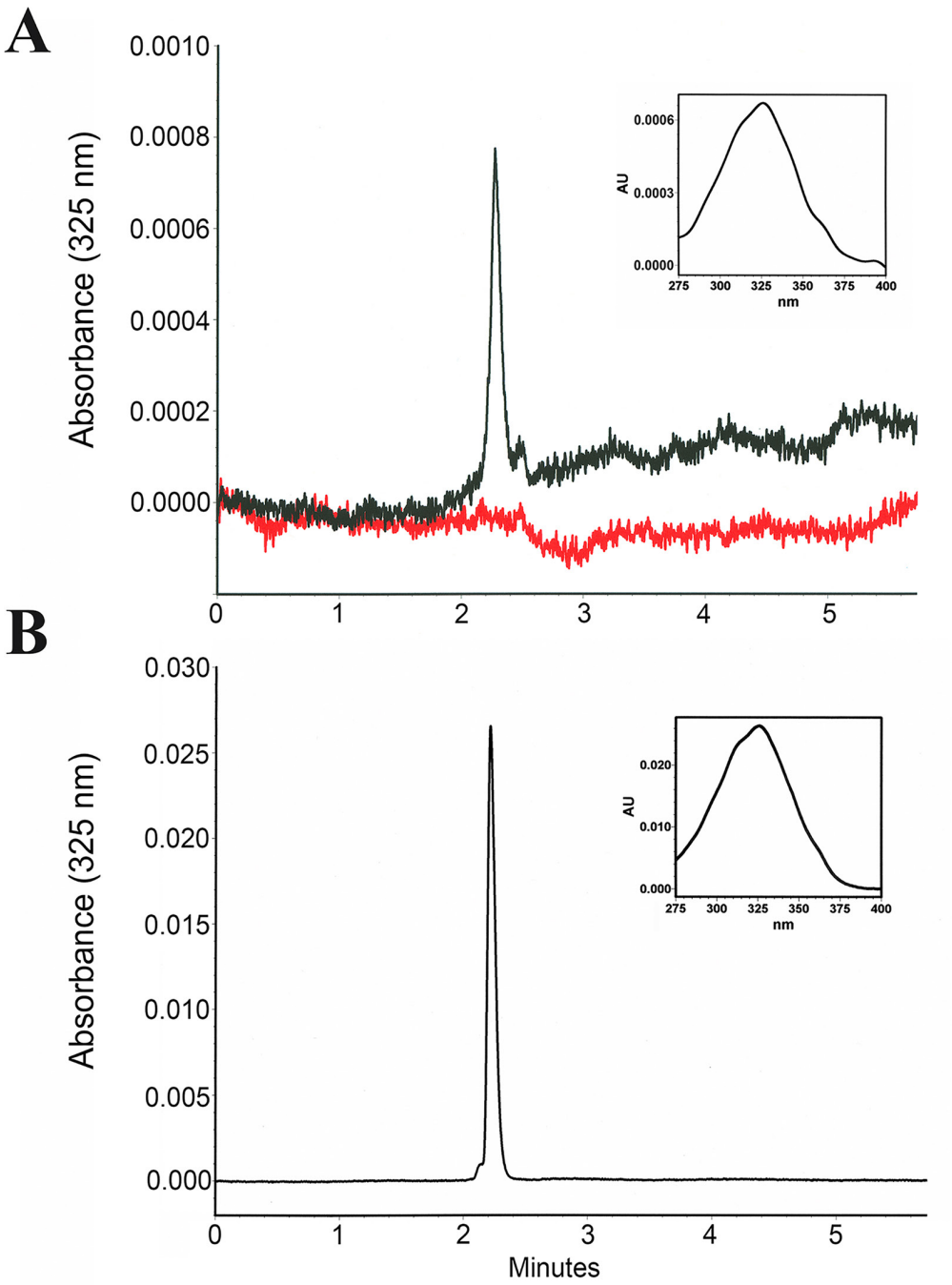

Figure 5. Retinyl ester synthesis in the differentiated ARPE-19 cells. Cells cultured for 4 months on Transwell® permeable membranes were incubated for 16 h with or without 4 μM all-*trans* retinol provided via the outside (basal) chamber. The cells were harvested, and the extracted retinoids were then analyzed with normal-phase high performance liquid chromatography (HPLC). **A**: Chromatogram overlay of retinoid extracts from ARPE-19 cells treated with (black) or without (red) all-*trans* retinol. The inset shows the absorbance spectrum from the peak observed in the treated ARPE-19 cells (black). **B**: Chromatogram of the authentic all-*trans* retinyl palmitate standard and its corresponding absorbance spectrum (inset).

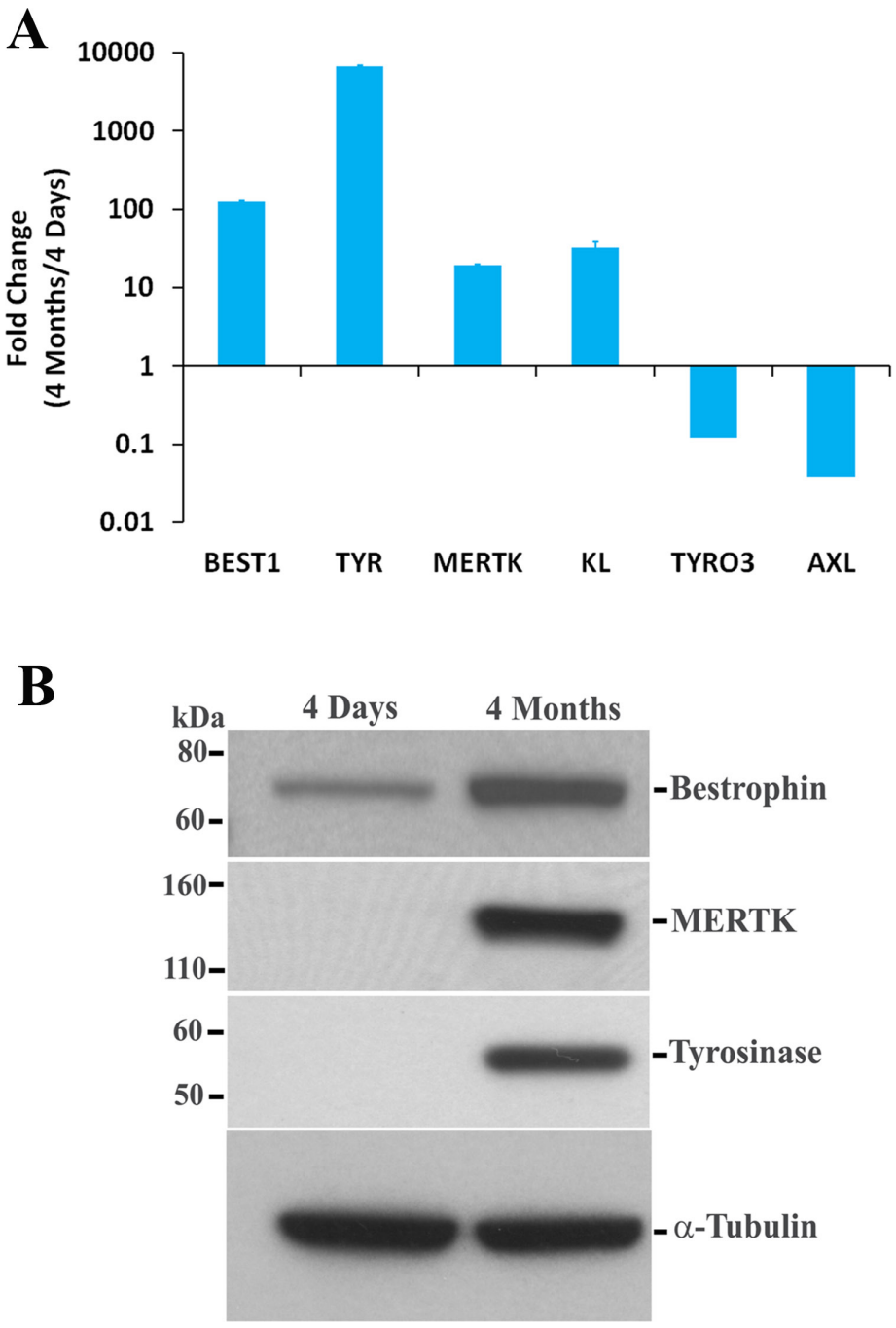

Figure 6. Differentiation of RPE cells increases non-visual cycle gene expression. ARPE-19 cells grown for either 4 days or 4 months were used for total RNA and protein extractions and were used for real-time quantitative PCR and western blotting, respectively, as described in the Methods section. **A**: Real-time PCR analysis of RPE-specific non-visual cycle mRNA expression. The values are mean ± standard deviation (SD), n = 4. *p<0.001 compared with control. **B**: Western blot analysis of the expression of the RPE-specific non-visual cycle proteins. α-Tubulin expression shows that the amount of protein used in different samples is similar.

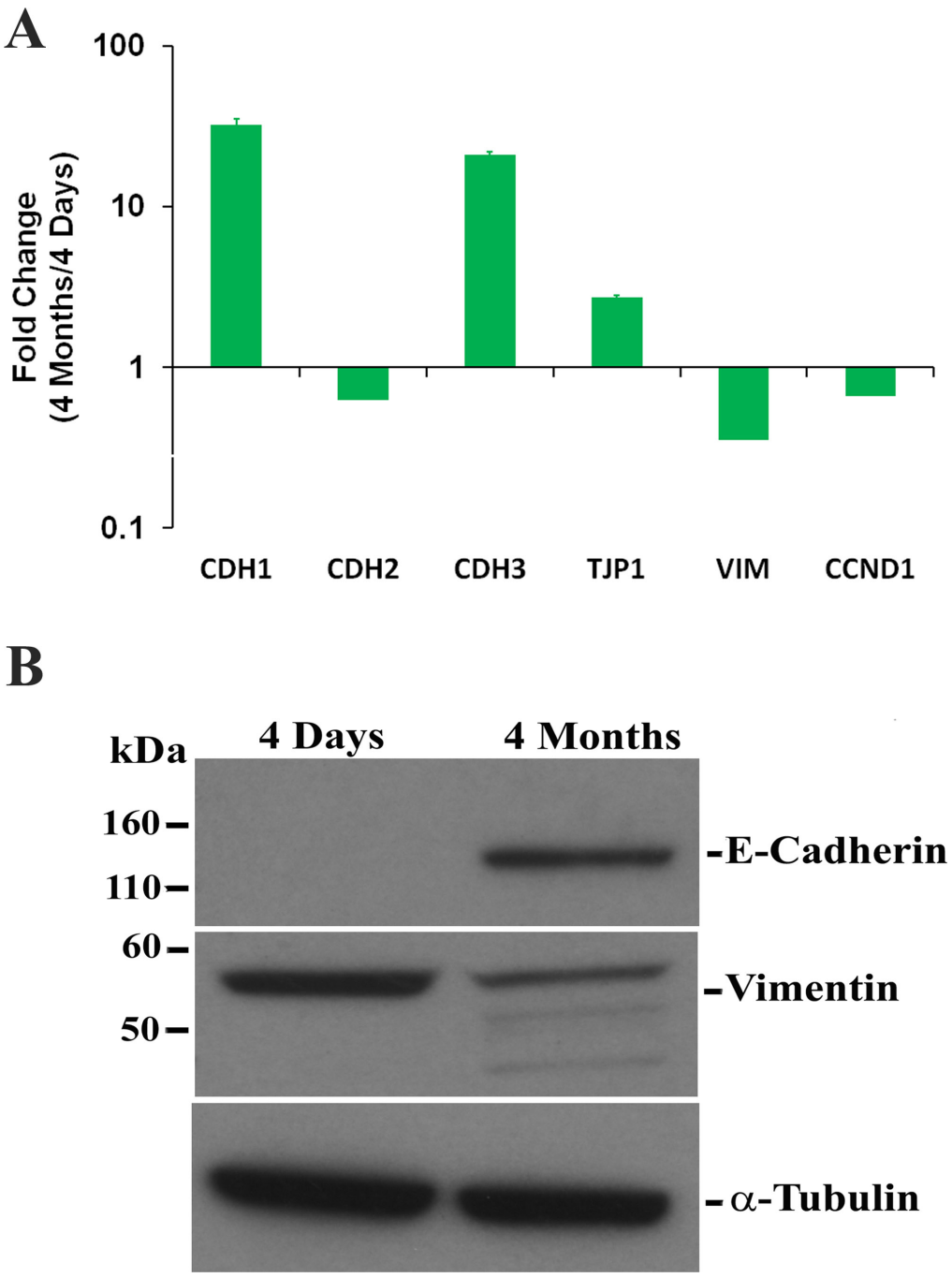

Figure 7. Epithelial-specific gene expression is increased in the differentiated ARPE-19 cells. ARPE-19 cells grown for either 4 days or 4 months were used for total RNA and protein extractions. The samples were then used for real-time quantitative PCR and western blotting, respectively, as described in the Methods section. **A**: Real-time PCR analysis of epithelial- and mesenchymal-specific mRNA expression. The values are mean ± standard deviation (SD), n = 4. *p<0.001 compared with control. **B**: Western blot analysis of the expression of the epithelial- and mesenchymal-specific proteins. α-Tubulin expression shows that the amount of protein used in different samples is similar.

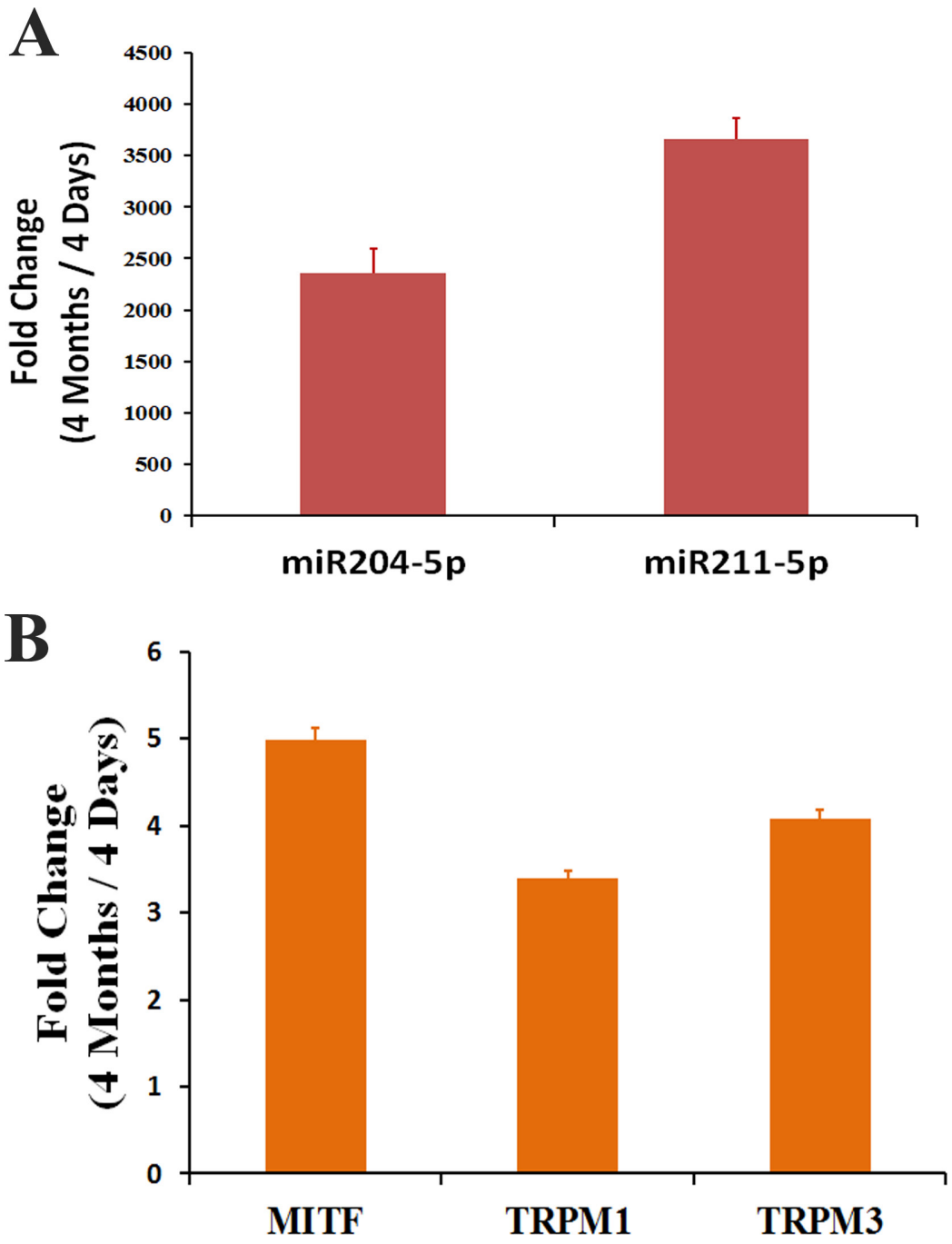

Figure 8. Expression of genes and miRNAs involved in regulating RPE differentiation is increased. ARPE-19 cells grown for either 4 days or 4 months were used for total RNA extractions. The samples were then used for real-time quantitative PCR, as described in the Methods section. **A**: Real-time PCR analysis of RPE-specific miRNAs, miR-204 and miR-211, expression. **B**: Real-time PCR analysis of *MITF* and its target genes *TRPM1* and *TRPM3* mRNA expression. The values are mean ± standard deviation (SD), n = 4. *p<0.001 compared with control.

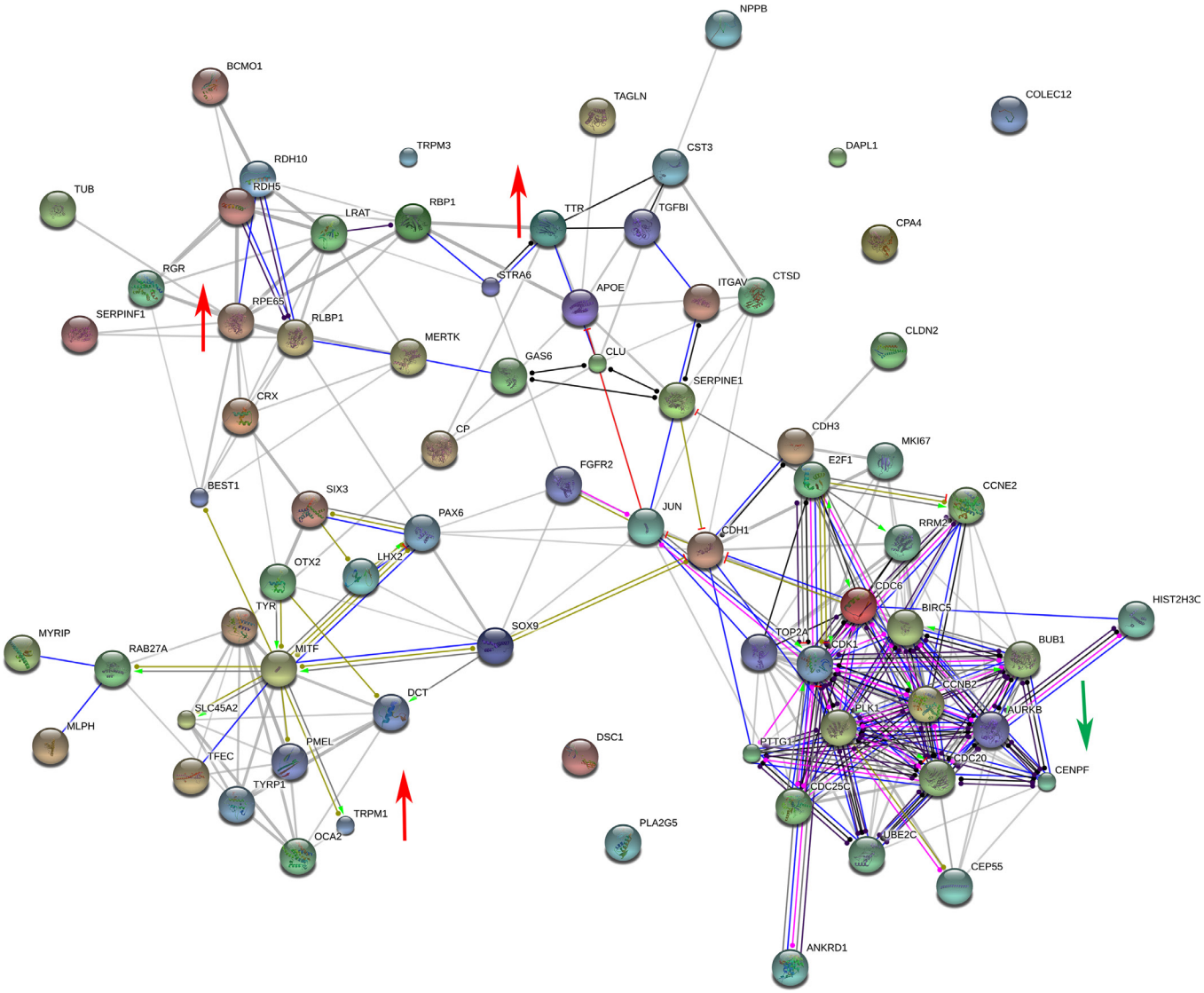

Figure 9. Protein network visualization of genes differentially expressed in the differentiated RPE cells. Significantly altered up- and downregulated genes were selected from the RNA sequencing (RNA-Seq) analysis of the RPE cells cultured for 4 days and for 4 months and were classified by their involvement in specific pathways. The STRING 10 database was used to visualize the known and predicted protein–protein interactions. Upregulated core set genes are indicated with red arrows and the downregulated genes with green arrows. The lines and arrows in different colors indicate the data sources: experimental (red), database (blue), and text-mining (green).

shown in Figure 8A, the ARPE-19 cells cultured for 4 months showed high expression of miR-204-5p and miR-211-5p. A more than 3,500-fold increase in miR-211-5p expression was observed in the cells cultured for 4 months compared with the cells cultured for 4 days, while miR-204-5p was increased by more than 2,000-fold. These data support our observation that the RPE cells grown for 4 months differentiated into an epithelial phenotype.

As miR-211 is contained within an intron of the transient receptor potential cation channel, subfamily m, member 1 (*TRPM1*) gene, and miR-204 is contained within an intron of the transient receptor potential cation channel, subfamily m, member 3 (*TRPM3*; OMIM 608961) gene, we measured the expression of *TRPM1* and *TRPM3* and found that both were highly increased in the ARPE-19 cells cultured for 4 months compared with the ARPE-19 cells cultured for 4 days (Figure 8B). *TRPM1* and *TRPM3* are regulated by MITF, therefore, it was not surprising that MITF expression was also greatly increased in the ARPE-19 cells cultured for 4 months compared with the ARPE-19 cells cultured for 4 days (Figure 8B).

Protein network visualization shows functional associations of differentially expressed genes: Potential interactions between the selected up- and downregulated differentially expressed genes from the RPE cells cultured for 4 months and 4 days were examined through STRING to determine associations between the differentially expressed genes. As shown in Figure 9, the network visualized in STRING illustrates that nearly all of the core gene set was organized into tight relationships among molecules; 67 of 72 genes were closely connected in a single network. The complex network could be segregated into four modules, involved in visual cycle, phagocytosis, melanin biosynthesis, and cell cycle regulation. The cell cycle regulation module contains polo-like kinase 1 (*PLK-1*; OMIM 602098), an early trigger for the G2/M transition [57], cyclin B2 (*CCNB2*; OMIM 602755), which plays a key role in TGFβ-mediated cell cycle control [58], and mitotic checkpoint serine/threonine-protein kinase BUB1 (*BUB1*; OMIM 602452), a central component of the mitotic checkpoint for spindle assembly (SAC) [59].

Differentiation increases RPE-specific gene expression: Previous studies have identified several specific genes that are preferentially expressed in human RPE compared to other tissues or cell types and suggested that they can be used to validate the progress of RPE differentiation and function [34,35]. Therefore, we performed a whole transcriptome comparison (> 20,000 genes) between the differentiated ARPE-19 cells data set and the reported transcriptomes from the hESC line–derived RPE (H1 and H9) and hfRPE isolated from 16-week gestation fetuses (HF) to determine the degree of similarity in gene expression [28]. For this analysis, we took the top 1,000 highly expressed genes from each transcriptome compared and calculated the extent of overlap with a Venn diagram analysis. When pooled, the four sets of 1,000 genes gave a union of 1,511 genes in total. The percentages shown in the Venn diagram were calculated by using this union of 1,511 genes as 100%. As shown in Figure 10A, we observed about 37% similarity (565 genes/1,511 total) in gene expression when these sets of genes from the cells cultured for 4 months and the transcriptomes of the H1, H9, and HF were compared. Similarly, we performed the same comparison with the analogous data sets from the HF and the native human RPE from the macular region of the RPE/choroid (RPE/CHOR_MAC). About a 23% (409 genes; union of 1,735 genes) overlap in gene expression was observed between the cells cultured for 4 months and of the HF and RPE/CHOR_MAC (Figure 10B). In terms of Gene Ontology, the number of GO biological pathway terms was significantly enriched in these 409 transcripts (data not shown). Significant terms included phagocytosis, melanin biosynthetic pathway, and vitamin A metabolism. In addition, based on the Spearman (measuring statistical dependence between the ranking of two variables; $S \geq 0.90$) and Pearson correlation coefficients (measuring the linear dependence between two variables; $R \geq 0.60$), the transcriptome of the ARPE-19 cells cultured for 4 months resembled more closely the HF than H1 or H9. However, the transcriptomes of H1 and H9 resembled each other more closely than the HF (Figure 10C–E). In addition, the Spearman correlation coefficients ($S \geq 0.79$ to 0.80) showed a high correlation between the RPE cells cultured for 4 months and the RPE cells isolated from the macular, nasal, and temporal regions of the RPE/choroid (Figure 10F–H). However, in the computation of the Pearson correlation coefficient ($R \geq 0.46$ to 0.39), weak correlation coefficients were observed between them.

To understand the functional similarities in terms of Gene Ontology, we compared 1,000 highly expressed genes from the data set and the RPE models from the hESCs and hfRPE, and native RPE from the macular regions of the RPE/choroid. The number of GO biological processes pathway terms was significantly enriched in these transcripts, and the top 18 are summarized in Table 4. Interestingly, of these 18 GO biological processes, four GO terms were highly increased (Yellow/Red, p-value ≥ 1.00E-06 to E-64) in all the data sets analyzed. Significant terms included translation and oxidative phosphorylation indicating that the most overrepresented pathways reflect the main property of metabolically active RPE cells. However, the levels of the mitochondrion-related process (electron transport, respiration, etc.) were low in the RPE cells cultured for 4 months and the HF (Blue, p-value ≤ 1.00E+00) compared to the native RPE. In addition, some GO biological processes are statistically significant only in the RPE models but not in the native tissue.

To explore genes that are preferentially expressed in human RPE, we assessed trends in gene expression across the data set of the ARPE-19 cells cultured for 4 months and the RNA-Seq data sets from the H1, H9, HF, and RPE from the macular, nasal, and temporal RPE/choroid punches. As shown in Figure 11A, the expression level of key visual cycle genes, such as *RPE65* and *LRAT*, was low in the ARPE-19 cells cultured for 4 months among all six samples analyzed, while the expression of *RLBP1* in the ARPE-19 cells cultured for 4 months was statistically significantly higher compared to that in the H1, H9, and HF. Significantly, the expression of *RPE65*, *RLBP1*, *RBP1*, *BEST1*, and *LRAT* was much higher in the native RPE cells compared to the H1, H9, and HF RPE cells. This indicates the high degree of functional enrichment in this set of genes in native tissue. When we cross-referenced the RNA-Seq data for several genes highly expressed in the native RPE (such as *SERPINF1*, *PMEL*, *TYR*, *MERTK*, and

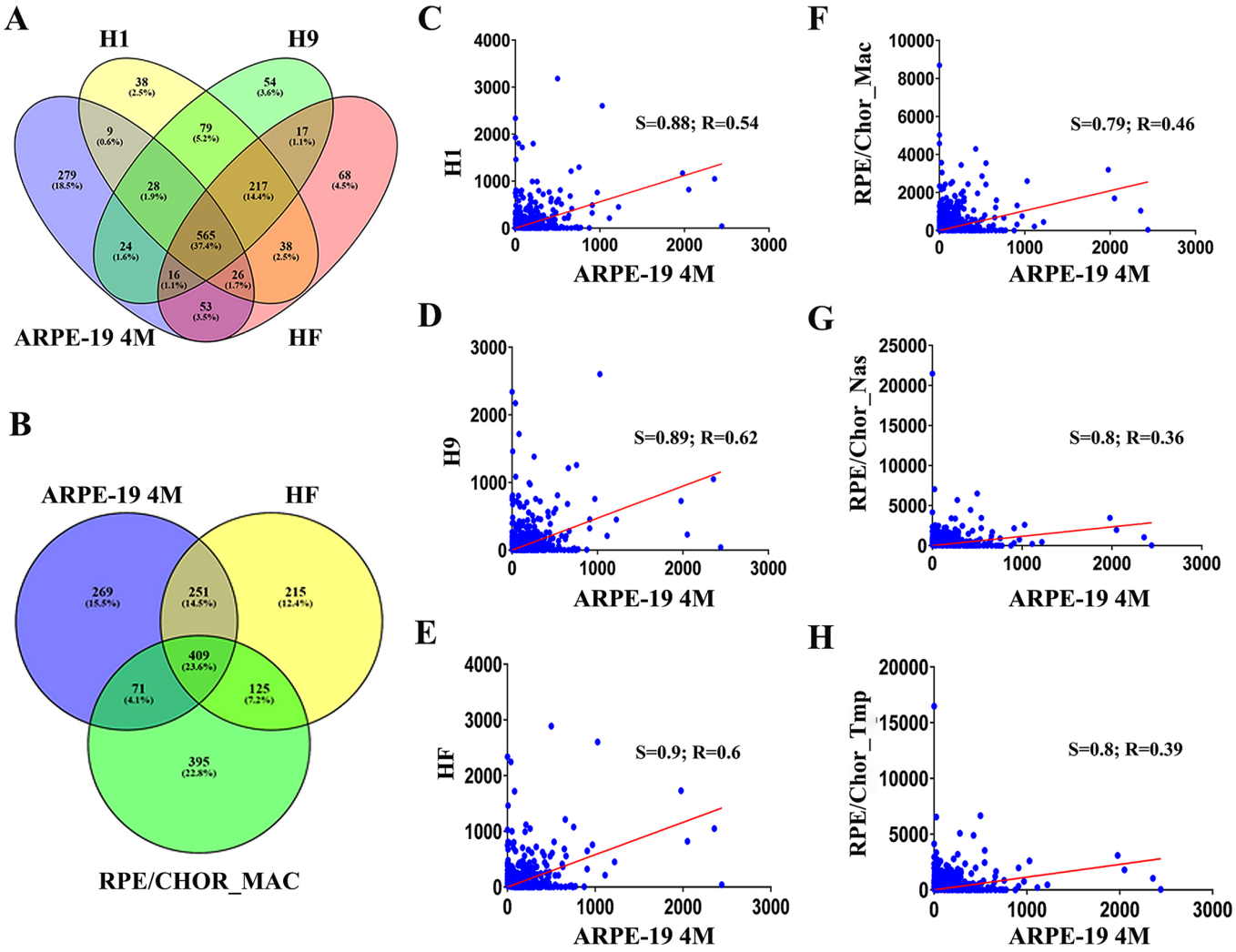

Figure 10. Comparative gene expression analysis between current RNA-Seq experiments and previous transcriptome studies of human primary and stem cell–derived RPE cells with RNAs sequencing (RNA-Seq). **A**: The Venn diagram shows the number of common and unique gene expression profiles between the 1,000 most highly expressed mRNA of the ARPE-19 cells cultured for 4 months (ARPE-19 4M) and RPE derived from human embryonic stem cells (H1 and H9) and fetal eyes (HF). The union of the four data sets gives rise to 1,511 genes, taken as the total for calculating the percentage shown. **B**: The Venn diagram shows the shared and unique genes among the 1,000 most highly expressed genes out of > 20,000 mRNA between the current RNA-Seq data (ARPE-19 4M), human embryonic stem cell-derived RPE cells (H1), and macular region of the RPE/choroid (RPE/CHOR_MAC). The union of these three data sets is 1,735 genes, taken as the total for calculating the percentages shown. **C**–**H**: Scatter plots with regression lines show the relations between each comparison. The regression line is in red. R = Pearson correlation coefficient; S = Spearman correlation coefficient. The x-axis corresponds to the gene expression observed in the ARPE-19 cells cultured for 4 months. The y-axis displays the RNA-Seq data set derived from the source.

MITF), we found these genes were highly expressed and even at levels similar to those of the native RPE cells (Figure 11B), corroborating the validity of the ARPE-19 cell differentiation phenotype.

DISCUSSION

In this paper, we show that, in addition to developing many of the structural and physiological properties characteristic of the native human RPE, long-term cultured ARPE-19 cells show an increase in genes preferentially expressed in the native RPE and epithelia. Gene Ontology analysis showed that in the cells cultured for 4 months the genes associated with visual cycle, phagocytosis, pigment synthesis, cell differentiation, and RPE-related transcription factors increased while the majority of the downregulated genes are associated with cell cycle and proliferation. Furthermore, this increase in the expression of the mRNA of the visual cycle and epithelial genes is translated into a corresponding increase in

protein expression. In addition, the two most RPE-enriched miRNAs and inducers of epithelial differentiation, miR-204 and miR-211, were increased in the RPE cells cultured for 4 months. Taken together, our data indicate that low-passage ARPE-19 cells grown for 4 months in DMEM + high glucose/pyruvate/1% FBS can be an important cell culture model for studying the physiology and pathophysiology of the native RPE in vitro.

ARPE-19 cells grown to sub-confluence or confluence for a short duration are the most commonly used system to study the RPE function in vitro. However, this presents a challenge to reproducibility as ARPE-19 cells adopt a variable phenotype depending upon the culture conditions [18,37,38,60]. Here, we showed that low-passage ARPE-19 cells grown in DMEM + high glucose/pyruvate/1% FBS for 4 months differentiated into a stable cobblestoned epithelial phenotype characteristic of native RPE in addition to reprising gene expression patterns commonly found in native RPE, primary RPE cultures, and hESC-derived RPE. In addition, heterogeneity and non-epithelial characteristics were not seen when ARPE-19 cells at passage numbers between 9 and 14 were used. Importantly, the study specifies that several months are required for the cultured cells to attain their epithelial phenotype after confluency, in common with various previous studies [5,18,22]. In this regard, lengthening the period of the in vitro cultures of induced pluripotent stem (iPS)-derived RPE cells to 18 weeks allowed for enhanced morphological differentiation [61]. Interestingly, even with extended culture, the composition of the medium is important to this differentiation process. Thus, ARPE-19 cells cultured similarly for 4 months in 1:1 DMEM and Ham's F12 (DMEM/F12) medium with high glucose and pyruvate supplemented with 1% FBS did not differentiate into an epithelial morphology (data not shown). This correlates well with the original report that ARPE-19 cells, even at higher passage numbers (22 to 28) differentiated into an epithelial phenotype when cultured in DMEM + high glucose/pyruvate/1% FBS for 3 months but did not in the typical DMEM/F12 medium with high glucose and pyruvate and 1% FBS [22].

In the present study, the expression of proteins that play a central role in inducing the epithelial phenotype was highly increased. In particular, cadherins (cell adhesion molecules that form adherens junctions) were highly increased in the ARPE-19 cells grown beyond confluency [62,63]. In

Table 4. Comparison of GO biological process between 4 months cultured ARPE-19 cells, primary human fetal RPE cells and native RPE from macular region of RPE/Choroid.

GO Biological Process	ARPE-19	HF	RPE\CHOR Macular
Translational elongation	6.80E-59[a]	2.00E-61[a]	3.90E-64[a]
Translation	3.30E-41[a]	1.30E-33[a]	2.80E-36[a]
Generation of precursor metabolites and energy	2.10E-14[a]	2.50E-08[a]	2.00E-21[a]
Oxidative phosphorylation	6.40E-09[a]	3.20E-06[b]	2.20E-15[a]
Electron transport chain	1.00E+00[c]	1.00E+00[c]	7.90E-10[a]
Cellular respiration	1.00E+00[c]	1.00E+00[c]	2.30E-07[a]
Mitochondrial electron transport, NADH to ubiquinone	1.00E+00[c]	1.00E+00[c]	4.80E-07[a]
Mitochondrial ATP synthesis coupled electron transport	1.00E+00[c]	1.00E+00[c]	1.00E-06[b]
Response to inorganic substance	1.00E+00[c]	1.80E-06[b]	9.40E-07[b]
Anti-apoptosis	1.00E+00[c]	1.20E-07[a]	7.00E-06[b]
Response to organic substance	1.00E+00[c]	7.80E-06[b]	4.00E-09[a]
Negative regulation of protein metabolic process	1.00E+00[c]	1.00E+00[c]	6.70E-09[a]
Oxidation reduction	3.30E-07[a]	1.00E+00[c]	8.00E-06[b]
Intracellular transport	2.30E-09[a]	9.90E-09[a]	1.00E+00[c]
Intracellular protein transport	2.60E-08[a]	1.60E-07[a]	1.00E+00[c]
Cellular protein localization	4.00E-08[a]	1.90E-07[a]	1.00E+00[c]
Cellular macromolecule localization	4.80E-08[a]	1.60E-07[a]	1.00E+00[c]
Protein localization	21.50E-06[b]	4.70E-06[b]	1.00E+00[c]

The table shows GO biological process common to the 1000 most highly expressed genes analyzed from RNA-Seq data of differentiated RPE cells and RPE cells from primary human fetal (HF) eye and macular region of native RPE/Choroid. p-value of 1 was assigned to pathways not overrepresented, and "a","b" and "c" denotes the changes in p-values; a < b < c

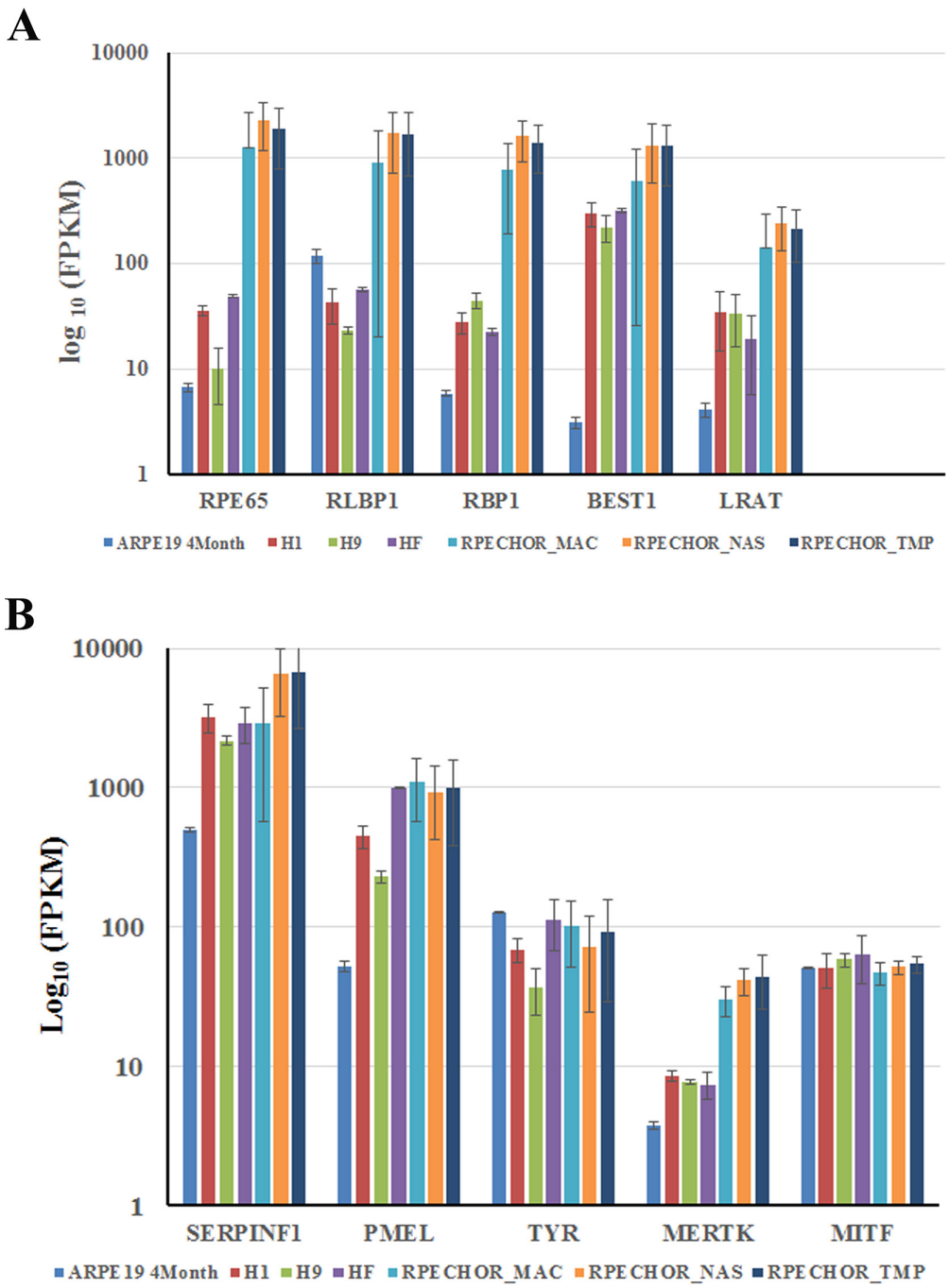

Figure 11. Comparison of visual cycle and RPE signature gene expression. Fragments per thousand bases of gene per million bases mapped (FPKM) values obtained from RNA sequencing (RNA-Seq) of the ARPE-19 cells cultured for 4 months (ARPE-19 4M), RPE derived from human embryonic stem cells (H1 and H9) and fetal eyes (HF), and native RPE from the nasal (RPE/CHOR_NAS), temporal (RPE/CHOR_TMP), and macular (RPE/CHOR_MAC) regions of the RPE/choroid were used for the analysis. **A**: Comparison of the expression of the visual cycle genes. **B**: Comparison of the expression of RPE-specific genes. The x-axis indicates the expression levels of the genes analyzed. The y-axis indicates the transcript expression levels quantified as FPKM on a $\log_{10}$ scale.

particular, the expression of E-cadherin (*CDH1*), a critical inducer of epithelial morphogenesis, was highly increased in the RPE cells cultured for 4 months compared with the cells cultured for 4 days. Western blot analysis showed that the E-cadherin protein was present only in the ARPE-19 cells cultured for 4 months, similar to an earlier observation that E-cadherin was detectable only in the cultures of primary human RPE cells maintained at confluence for several weeks [53]. Furthermore, an increase in P-cadherin (*CDH3*) expression, an epithelial cadherin coexpressed with E-cadherin and required for human RPE viability [53,64], in the cells cultured for 4 months further correlates with the observed epithelial phenotype. N-cadherin (*CDH2*), typically found in nonepithelial cells, was decreased in the cells cultured for 4 months, consistent with the reduced coexpression of N-cadherin with E-cadherin [65]. However, epithelial cells have an inherent plasticity to transition into mesenchymal cells (e.g., fibroblasts) via EMT, and back to epithelia via mesenchymal to epithelial transition (MET), either fully or partially [19]. The expression of vimentin, a canonical mesenchymal indicator, was markedly decreased in the ARPE-19 cells cultured for 4 months suggesting that MET may mediate the epithelial differentiation. The decrease in vimentin protein in the cells cultured for 4 months underscores the loss by the cells of their migratory property and their acquisition of polarity and expression of tight junction protein ZO-1, a structural feature of native RPE monolayers. However, downregulation of *ZO-1* and E-cadherin expression by *TGF-β* in ARPE-19 cells has been associated with EMT [66,67]. Correspondingly, we found that *TGF-β* expression was downregulated in the ARPE-19 cells cultured for 4 months, further supporting a role for MET in the epithelial phenotype differentiation. In addition, we observed with immunofluorescence microscopy that claudin-2, a minor tight junction protein, colocalizes with *ZO-1* uniformly across the monolayer in the differentiated ARPE-19 cells. It is known that the formation of tight junctions is an essential component of the epithelial monolayer barrier formation [68]. However, modulation of the RPE tight junction by minor claudins needs further evaluation to understand the mechanism through which they might regulate the barrier properties [69,70]. Recently, it has been shown that overexpression of either claudin-3 or claudin-19, the major claudins in native human RPE, improved the barrier function, increased the expression of genes related to RPE, and partially restored native RPE phenotype to high-passage ARPE-19 cells cultured for 2 weeks [71]. Whether these phenomena could be observed in the differentiated ARPE-19 cells needs further investigation.

In addition to developing the typical cobblestoned morphology of native RPE, the ARPE-19 cells cultured for 4 months were heavily pigmented to the naked eye. Pigmentation is a hallmark of native human RPE, and an important indicator of phenotypic maturity of these cells in culture [72,73], requiring functional melanosomes containing melanogenesis enzymes, including tyrosinase (*TYR*), tyrosinase-related protein (*TYRP1*), and L-dopachrome tautomerase (*DCT*). Although melanin pigments occur in human fetal RPE cultures [7,9], the most common phenotype deficiency of immortalized adult human RPE cells has been the lack of melanin biosynthesis under common culture conditions [50]. In the present study, mRNA and protein expression of tyrosinase, PMEL, a key component of mammalian melanosome biogenesis, and DCT, which helps to regulate eumelanin and pheomelanin levels [39], were all highly increased in the ARPE-19 cells cultured for 4 months. The present results are in contrast to earlier observations that melanogenesis occurs more reliably in cultured fetal RPE cells [9,74]. Specialized media or substrates have been shown to play a role in inducing melanogenesis and differentiation. In particular, pyruvate has been reported to increase pigmentation in non-RPE cells [75,76].

We grew ARPE-19 cells on plastic as ARPE-19 cells grown on a plastic surface have a closer expression profile to native RPE than cells grown on protein matrices [36]. We used RNA-Seq as it allows for greater sensitivity and a broader range of fold changes than microarrays. The most highly upregulated genes included *RPE65*, *DCT*, and *DAPL1*. However, many downregulated genes are involved in cell cycle, proliferation, and transcription factors that play a central role in cell cycle and apoptosis. The presence of *RPE65* [77-79] is of particular importance as this gene plays a critical role in the retinoid cycle and is a marker for terminally differentiated RPE cells. Even then, while the mRNA expression of *RPE65* was highly increased (about 10,000 fold), we were unable to detect the RPE65 protein in these cells. This result is consistent with numerous studies that have demonstrated *RPE65* mRNA in ARPE-19 cells with no detectable level of the RPE65 protein [5,38,60]. A decrease in the RPE65 protein was also observed in the primary cultures of monkey and bovine [12] RPE cells. In contrast, Ahamado et al. [22] observed the RPE65 protein in addition to RPE65 mRNA in ARPE-19 cells cultured for 3 months in DMEM + high glucose/pyruvate/1% FBS. Other than *RPE65*, the increased expression of other visual cycle genes [1], *LRAT*, *RDH5*, and *RLBP1* also known as *CRALBP* (retinaldehyde-binding protein 1), correlated with increases in protein expression, confirming the degree of differentiation of the ARPE-19 cells cultured for 4 months. In addition, the expression of bestrophin-1, another important marker of terminal RPE maturation [80], was highly increased in the ARPE-19 cells

cultured for 4 months, and the increase was translated to a corresponding increase in the protein. Previously, the bestrophin-1 protein had been shown to accumulate only in cells of fetal origin [9,74]. A recent study also showed a more than fourfold increase in bestrophin-1 mRNA expression when the ARPE-19 cells grown for 2 weeks were transfected exogenously with either claudin-3 or claudin-19 [71]. However, the observed increase in *BEST1* mRNA expression was not translated into a corresponding increase in the bestrophin-1 protein [71].

It is evident from these observations that ARPE-19 cells grown for 4 months in DMEM + high glucose/pyruvate/1% FBS express proteins, except RPE65, that play a central role in the classical retinoid visual cycle performed by the RPE, a signature feature of the RPE monolayer [81]. This is in line with observations that RPE culture conditions can be crucial for the expression of proteins essential for the retinoid visual cycle [82]. However, it has been shown earlier that RPE can be morphologically normal but lack the essential activity of LRAT, the sole enzyme responsible for RPE retinyl ester formations needed for vitamin A storage and as the substrate for the isomerase of the visual cycle [82,83]. Here we observed that the ARPE-19 cells grown on Transwell® inserts for 4 months developed morphology approximating that of the native RPE and are able to synthesize all-*trans* retinyl esters from all-*trans* retinol provided in the basal chamber, indicative of an active LRAT enzyme. Accumulation of all-*trans* retinyl ester with no detectable 11-*cis* retinal is attributed to the lack of the RPE65 protein. This may be due to post-transcriptional regulation of RPE65 expression during cell culture as previously described [12].

Another important function of RPE is the daily phagocytosis and clearance of shed POS disks [84]. Phagocytosis by RPE cells in culture is highly dependent on the expression of the RPE phagocytosis molecular machinery and on the degree of RPE differentiation or polarization. We found that several genes implicated in phagocytosis were highly increased in the differentiated ARPE-19 cells, including *integrin alpha-V*, *cathepsin D*, and *MERTK*, and confirmed the expression of the MERTK protein with western blotting. Integrins (integral membrane proteins that function as an αβ heterodimer), present in the apical surface of the RPE, are responsible for POS binding to the RPE [14]. Mice or rats lacking αvβ5 integrin or *Mertk* have profound abnormalities in cytosolic phagocytic signaling with severely reduced POS binding and engulfment [40,85-88]. The expression level of *MERTK* also plays an important role in mediating phagocytosis in human primary RPE cells [51]. Furthermore, cathepsin D, a major lysosomal enzyme that degrades internalized POS, was also increased in the differentiated ARPE-19 cells cultured for 4 months. Thus, taken together these data indicate that the ARPE-19 cells cultured for 4 months are competent to phagocytose and degrade POS in vitro.

Cell differentiation requires highly regulated gene expression mediated by specific transcription factors. We saw increases in several transcription factors known to promote differentiation, survival, proliferation, and melanogenesis in RPE. Transcription factor EC (TFEC), belonging to the family of basic helix-loop-helix-zipper transcription factors, such as MITF, TFE3, and TFEB, was highly increased in the ARPE-19 cells cultured for 4 months. TFEC regulates osteoclast differentiation in mice, forming heterodimers with MITF to activate target genes [89]. Apart from binding to TFEC, MITF stimulates the expression of its target genes as a homodimer or through cross-regulation with transcription factors, such as PAX6, OTX2, and SOX9 [90], considered the key regulators for RPE specification together with MITF. We found increased expression of the *KL* gene that is expressed in primary cultured human RPE and that regulates MITF and TYR, further supporting the similarities of differentiated ARPE-19 cells to primary human RPE cells. Further, the mRNA expression of *TRPM1* and *TRPM3*, tightly controlled by MITF, was highly increased in the differentiated RPE cells. MITF also regulates the transcription of melanogenesis genes (including *TYR*, *TRP1*, and *DCT*) and synergistically interacts with OTX2 and SOX9, both increased in differentiated ARPE-19 cells, to activate the transcription of several visual cycle genes [44]. Thus, MITF together with OTX2, PAX6, and SOX6 may be responsible for the changes (synthesis of melanin, epithelial phenotype differentiation, and upregulation of the RPE-specific genes) in these cells. The potential interactions between the up- and downregulated genes visualized in the STRING action view (Figure 9) also illustrates that nearly all of the core gene set was organized into tight relationships among the molecules (visual cycle, phagocytosis, melanogenesis, and cell cycle regulation) underlying the differentiation.

In addition to transcriptional control, regulation of mRNA translation by miRNA presents yet another level of regulation that affects cell fate and various biologic processes. RPE-specific miRNAs could be involved in RPE maturation related to the expression of genes involved in the visual cycle pathway and pigmentation [91,92]. Using microarray analysis, our laboratory showed that many miRNAs with the inherent ability to regulate cell growth, differentiation, and development are normally expressed in ARPE-19 cells [93]. Wang et al. [8] showed that miR-204 and -211 are the two most highly expressed miRNAs in primary cultures of human fetal RPE

and play a critical role in maintaining epithelial barrier function and cell physiology. Adijanto et al. showed directly that transfection of pre-miR-204/211 into hfRPE cells promoted differentiation, while the addition of miR-204/211 inhibitors caused dedifferentiation [56]. We found that the expression of miR-204 and miR-211 were greatly increased in the ARPE-19 cultured for 4 months, suggesting the involvement of miR-204/211 in mediating its differentiation.

Finally, we compared the RNA-Seq data set to two previously reported transcriptome analyses of RPE cells, one of RPE derived from hESCs and hfRPE and the other of native RPE isolated from the macular, nasal, and temporal regions of the RPE/choroid [26,28]. This comparison is of interest because these RNA-Seq data sets can provide potential molecular markers for assessing the integrity and function of RPE and to validate the progress of RPE differentiation [35]. There is about 37% (565 genes; union of 1,511 genes) similarity in gene expression between the ARPE-19 RNA-Seq data and the transcriptome analyses of hESCs and hfRPE. When compared with the RNA-Seq data for the macular regions of the RPE/choroid and hfRPE, there was a 23% (409 genes; union of 1,735 genes) similarity in gene expression. Gene Ontology analysis indicated that included among these genes were visual cycle proteins, epithelial markers, and transporters, such as *RPE65*, *RBP1*, *BEST1*, *CDH3*, and *SLC6A20*. This indicates that, in addition to morphology, the transcriptome of the differentiated ARPE-19 cells resembles that of other reported RNA-Seq derived expression data sets. Although significant similarity in gene expression was observed between all cell culture models, the absolute expression values of the genes specific to RPE functions were quite low compared to that of native RPE. In particular, the expression values of the genes involved in the RPE part of the visual cycle were comparatively greatly decreased even in hfRPE, considered a well-regarded model of RPE function, compared with native RPE. It is possible that the observed difference in gene expression could be due to mitochondrial dysfunction associated with cultured RPE cells. The GO biological process comparison showed low expression of the genes related to mitochondrial function in the cultured RPE cells compared with the native RPE. Mitochondrial dysfunction resulted in a shift in cell metabolism and was accompanied by the loss of RPE-specific genes [94]. In addition, we cannot rule out that the relative lack of maturity of the RPE cells derived from either stem cell or fetal RPE compared to native adult RPE is another possible reason for the observed differences in gene expression. This possibility is supported by an earlier observation that the RPE transcriptome dynamically changes during the outer blood–retinal barrier development [95]. However, the moderate difference observed between the ARPE-19 cells cultured for 4 months with the hESC-derived RPE and primary hfRPE cells is not unexpected considering the experimental design and the differences in the culture conditions used in the respective analyses. In addition, it is possible that the observed difference could be due to the ARPE-19 cells being grown on a plastic surface as it has been shown that human fetal RPE cells grown on Transwell® filters produce confluent RPE with morphological and physiological characteristics of the intact RPE monolayer [9]. However, irregular morphology in hESC-derived RPE cells has been observed in human extracellular matrix-coated Transwell® filters that promoted differentiation of hfRPE [28]. RPE cells grown on a plastic surface were shown previously to have a closer expression profile to native RPE than cells grown on protein matrices [36].

In summary, our study provides a detailed description of RPE-specific gene expression in differentiated ARPE-19 cells. Most importantly, our data reveal a striking similarity in overall gene expression between these ARPE-19 cells and primary and native human RPE cells, indicating that well-differentiated ARPE-19 cells can provide a useful tool for studying different RPE cellular functions in vitro. This study also showed the increased expression of important proteins normally found in the RPE, including visual cycle proteins, in the differentiated ARPE-19 cells. Surprisingly, however, the RPE65 protein was undetectable even in the fully differentiated cells, despite the abundant RPE65 mRNA expression. Given this level of functionality, it is apparent that culture conditions are crucial to gene expression profiles. Although care must be used when interpreting and extrapolating gene expression changes between cultured and native RPE cells, we conclude that appropriately cultured and differentiated low-passage ARPE-19 cells can be functional models for RPE studies. Finally, the results observed for the low-passaged ARPE-19 cells can be used as a standard for comparison for cultures of late passage ARPE-19 cells.

ACKNOWLEDGMENTS

This study was supported by the Intramural Research Program of the National Eye Institute, NIH.

REFERENCES

1. Strauss O. The retinal pigment epithelium in visual function. Physiol Rev 2005; 85:845-81. [PMID: 15987797].

2. Bhutto I, Lutty G. Understanding age-related macular degeneration (AMD): relationships between the photoreceptor/retinal pigment epithelium/Bruch's membrane/choriocapillaris complex. Mol Aspects Med 2012; 33:295-317. [PMID: 22542780].

3. Phelan JK, Bok D. A brief review of retinitis pigmentosa and the identified retinitis pigmentosa genes. Mol Vis 2000; 6:116-24. [PMID: 10889272].

4. Greenwood J, Pryce G, Devine L, Male DK, dos Santos WL, Calder VL, Adamson P. SV40 large T immortalised cell lines of the rat blood-brain and blood-retinal barriers retain their phenotypic and immunological characteristics. J Neuroimmunol 1996; 71:51-63. [PMID: 8982103].

5. Dunn KC, Aotaki-Keen AE, Putkey FR, Hjelmeland LM. ARPE-19, a human retinal pigment epithelial cell line with differentiated properties. Exp Eye Res 1996; 62:155-69. [PMID: 8698076].

6. Toops KA, Tan LX, Lakkaraju A. A detailed three-step protocol for live imaging of intracellular traffic in polarized primary porcine RPE monolayers. Exp Eye Res 2014; 124:74-85. [PMID: 24861273].

7. Hu J, Bok D. A cell culture medium that supports the differentiation of human retinal pigment epithelium into functionally polarized monolayers. Mol Vis 2001; 7:14-9. [PMID: 11182021].

8. Wang FE, Zhang C, Maminishkis A, Dong L, Zhi C, Li R, Zhao J, Majerciak V, Gaur AB, Chen S, Miller SS. MicroRNA-204/211 alters epithelial physiology. FASEB J 2010; 24:1552-71. [PMID: 20056717].

9. Maminishkis A, Chen S, Jalickee S, Banzon T, Shi G, Wang FE, Ehalt T, Hammer JA, Miller SS. Confluent monolayers of cultured human fetal retinal pigment epithelium exhibit morphology and physiology of native tissue. Invest Ophthalmol Vis Sci 2006; 47:3612-24. [PMID: 16877436].

10. Stern JH, Temple S. Stem cells for retinal replacement therapy. Neurotherapeutics 2011; 8:736-43. [PMID: 21948217].

11. Adijanto J, Philp NJ. Cultured primary human fetal retinal pigment epithelium (hfRPE) as a model for evaluating RPE metabolism. Exp Eye Res 2014; 126:77-84. [PMID: 24485945].

12. Hamel CP, Tsilou E, Pfeffer BA, Hooks JJ, Detrick B, Redmond TM. Molecular cloning and expression of RPE65, a novel retinal pigment epithelium-specific microsomal protein that is post-transcriptionally regulated in vitro. J Biol Chem 1993; 268:15751-7. [PMID: 8340400].

13. Eisenfeld AJ, Bunt-Milam AH, Saari JC. Localization of retinoid-binding proteins in developing rat retina. Exp Eye Res 1985; 41:299-304. [PMID: 3905423].

14. Finnemann SC, Bonilha VL, Marmorstein AD, Rodriguez-Boulan E. Phagocytosis of rod outer segments by retinal pigment epithelial cells requires alpha(v)beta5 integrin for binding but not for internalization. Proc Natl Acad Sci USA 1997; 94:12932-7. [PMID: 9371778].

15. Alizadeh M, Wada M, Gelfman CM, Handa JT, Hjelmeland LM. Downregulation of differentiation specific gene expression by oxidative stress in ARPE-19 cells. Invest Ophthalmol Vis Sci 2001; 42:2706-13. [PMID: 11581219].

16. Chen S, Samuel W, Fariss RN, Duncan T, Kutty RK, Wiggert B. Differentiation of human retinal pigment epithelial cells into neuronal phenotype by N-(4-hydroxyphenyl)retinamide. J Neurochem 2003; 84:972-81. [PMID: 12603822].

17. Zhang C, Baffi J, Cousins SW, Csaky KG. Oxidant-induced cell death in retinal pigment epithelium cells mediated through the release of apoptosis-inducing factor. J Cell Sci 2003; 116:1915-23. [PMID: 12668724].

18. Luo Y, Zhuo Y, Fukuhara M, Rizzolo LJ. Effects of culture conditions on heterogeneity and the apical junctional complex of the ARPE-19 cell line. Invest Ophthalmol Vis Sci 2006; 47:3644-55. [PMID: 16877439].

19. Kalluri R, Weinberg RA. The basics of epithelial-mesenchymal transition. J Clin Invest 2009; 119:1420-8. [PMID: 19487818].

20. Diaz-Lopez A, Moreno-Bueno G, Cano A. Role of microRNA in epithelial to mesenchymal transition and metastasis and clinical perspectives. Cancer Manag Res 2014; 6:205-16. [PMID: 24812525].

21. Gregory PA, Bert AG, Paterson EL, Barry SC, Tsykin A, Farshid G, Vadas MA, Khew-Goodall Y, Goodall GJ. The miR-200 family and miR-205 regulate epithelial to mesenchymal transition by targeting ZEB1 and SIP1. Nat Cell Biol 2008; 10:593-601. [PMID: 18376396].

22. Ahmado A, Carr AJ, Vugler AA, Semo M, Gias C, Lawrence JM, Chen LL, Chen FK, Turowski P, da Cruz L, Coffey PJ. Induction of differentiation by pyruvate and DMEM in the human retinal pigment epithelium cell line ARPE-19. Invest Ophthalmol Vis Sci 2011; 52:7148-59. [PMID: 21743014].

23. Poliakov E, Strunnikova NV, Jiang JK, Martinez B, Parikh T, Lakkaraju A, Thomas C, Brooks BP, Redmond TM. Multiple A2E treatments lead to melanization of rod outer segment-challenged ARPE-19 cells. Mol Vis 2014; 20:285-300. [PMID: 24644403].

24. Love MI, Huber W, Anders S. Moderated estimation of fold change and dispersion for RNA-seq data with DESeq2. Genome Biol 2014; 15:550-[PMID: 25516281].

25. Subramanian A, Tamayo P, Mootha VK, Mukherjee S, Ebert BL, Gillette MA, Paulovich A, Pomeroy SL, Golub TR, Lander ES, Mesirov JP. Gene set enrichment analysis: a knowledge-based approach for interpreting genome-wide expression profiles. Proc Natl Acad Sci USA 2005; 102:15545-50. [PMID: 16199517].

26. Whitmore SS, Wagner AH, DeLuca AP, Drack AV, Stone EM, Tucker BA, Zeng S, Braun TA, Mullins RF, Scheetz TE. Transcriptomic analysis across nasal, temporal, and macular regions of human neural retina and RPE/choroid by RNA-Seq. Exp Eye Res 2014; 129:93-106. [PMID: 25446321].

27. . Huang W. Sherman BT, Lempicki RA. Systematic and integrative analysis of large gene lists using DAVID bioinformatics resources. Nat Protoc 2009; 4:44-57. [PMID: 19131956].

28. Peng S, Gan G, Qiu C, Zhong M, An H, Adelman RA, Rizzolo LJ. Engineering a blood-retinal barrier with human embryonic stem cell-derived retinal pigment epithelium:

transcriptome and functional analysis. Stem Cells Transl Med 2013; 2:534-44. [PMID: 23734062].

29. Garwin GG, Saari JC. High-performance liquid chromatography analysis of visual cycle retinoids. Methods Enzymol 2000; 316:313-24. [PMID: 10800683].

30. Franceschini A, Szklarczyk D, Frankild S, Kuhn M, Simonovic M, Roth A, Lin J, Minguez P, Bork P, von Mering C, Jensen LJ. STRING v9.1: protein-protein interaction networks, with increased coverage and integration. Nucleic Acids Res 2013; 41:D808-15. [PMID: 23203871].

31. Grisanti S, Guidry C. Transdifferentiation of retinal pigment epithelial cells from epithelial to mesenchymal phenotype. Invest Ophthalmol Vis Sci 1995; 36:391-405. [PMID: 7531185].

32. Madara JL. Regulation of the movement of solutes across tight junctions. Annu Rev Physiol 1998; 60:143-59. [PMID: 9558458].

33. Rizzolo LJ, Peng S, Luo Y, Xiao W. Integration of tight junctions and claudins with the barrier functions of the retinal pigment epithelium. Prog Retin Eye Res 2011; 30:296-323. [PMID: 21704180].

34. Booij JC, ten Brink JB, Swagemakers SM, Verkerk AJ, Essing AH, van der Spek PJ, Bergen AA. A new strategy to identify and annotate human RPE-specific gene expression. PLoS One 2010; 5:e9341-[PMID: 20479888].

35. Strunnikova NV, Maminishkis A, Barb JJ, Wang F, Zhi C, Sergeev Y, Chen W, Edwards AO, Stambolian D, Abecasis G, Swaroop A, Munson PJ, Miller SS. Transcriptome analysis and molecular signature of human retinal pigment epithelium. Hum Mol Genet 2010; 19:2468-86. [PMID: 20360305].

36. Tian J, Ishibashi K, Handa JT. The expression of native and cultured RPE grown on different matrices. Physiol Genomics 2004; 17:170-82. [PMID: 14982971].

37. Cai H, Del Priore LV. Gene expression profile of cultured adult compared to immortalized human RPE. Mol Vis 2006; 12:1-14. [PMID: 16446697].

38. Tian J, Ishibashi K, Honda S, Boylan SA, Hjelmeland LM, Handa JT. The expression of native and cultured human retinal pigment epithelial cells grown in different culture conditions. Br J Ophthalmol 2005; 89:1510-7. [PMID: 16234463].

39. Körner AM, Pawelek J. Dopachrome conversion: a possible control point in melanin biosynthesis. J Invest Dermatol 1980; 75:192-5. [PMID: 6774031].

40. Feng W, Yasumura D, Matthes MT, LaVail MM, Vollrath D. Mertk triggers uptake of photoreceptor outer segments during phagocytosis by cultured retinal pigment epithelial cells. J Biol Chem 2002; 277:17016-22. [PMID: 11861639].

41. Finnemann SC, Nandrot EF. MerTK activation during RPE phagocytosis in vivo requires alphaVbeta5 integrin. Adv Exp Med Biol 2006; 572:499-503. [PMID: 17249615].

42. Sun L, Ryan DG, Zhou M, Sun TT, Lavker RM. EEDA: a protein associated with an early stage of stratified epithelial differentiation. J Cell Physiol 2006; 206:103-11. [PMID: 15920738].

43. Raviv S, Bharti K, Rencus-Lazar S, Cohen-Tayar Y, Schyr R, Evantal N, Meshorer E, Zilberberg A, Idelson M, Reubinoff B, Grebe R, Rosin-Arbesfeld R, Lauderdale J, Lutty G, Arnheiter H, Ashery-Padan R. PAX6 regulates melanogenesis in the retinal pigmented epithelium through feed-forward regulatory interactions with MITF. PLoS Genet 2014; 10:e1004360-[PMID: 24875170].

44. Masuda T, Wahlin K, Wan J, Hu J, Maruotti J, Yang X, Iacovelli J, Wolkow N, Kist R, Dunaief JL, Qian J, Zack DJ, Esumi N. Transcription factor SOX9 plays a key role in the regulation of visual cycle gene expression in the retinal pigment epithelium. J Biol Chem 2014; 289:12908-21. [PMID: 24634209].

45. Martinez-Morales JR, Signore M, Acampora D, Simeone A, Bovolenta P. Otx genes are required for tissue specification in the developing eye. Development 2001; 128:2019-30. [PMID: 11493524].

46. Tsukiji N, Nishihara D, Yajima I, Takeda K, Shibahara S, Yamamoto H. Mitf functions as an in ovo regulator for cell differentiation and proliferation during development of the chick RPE. Dev Biol 2009; 326:335-46. [PMID: 19100253].

47. Mochii M, Mazaki Y, Mizuno N, Hayashi H, Eguchi G. Role of Mitf in differentiation and transdifferentiation of chicken pigmented epithelial cell. Dev Biol 1998; 193:47-62. [PMID: 9466887].

48. Nawshad A, Lagamba D, Polad A, Hay ED. Transforming growth factor-beta signaling during epithelial-mesenchymal transformation: implications for embryogenesis and tumor metastasis. Cells Tissues Organs 2005; 179:11-23. [PMID: 15942189].

49. Bakall B, Marmorstein LY, Hoppe G, Peachey NS, Wadelius C, Marmorstein AD. Expression and localization of bestrophin during normal mouse development. Invest Ophthalmol Vis Sci 2003; 44:3622-8. [PMID: 12882816].

50. Reinisalo M, Putula J, Mannermaa E, Urtti A, Honkakoski P. Regulation of the human tyrosinase gene in retinal pigment epithelium cells: the significance of transcription factor orthodenticle homeobox 2 and its polymorphic binding site. Mol Vis 2012; 18:38-54. [PMID: 22259223].

51. Kokkinaki M, Abu-Asab M, Gunawardena N, Ahern G, Javidnia M, Young J, Golestaneh N. Klotho regulates retinal pigment epithelial functions and protects against oxidative stress. J Neurosci 2013; 33:16346-59. [PMID: 24107965].

52. Tsou WI, Nguyen KQ, Calarese DA, Garforth SJ, Antes AL, Smirnov SV, Almo SC, Birge RB, Kotenko SV. Receptor tyrosine kinases, TYRO3, AXL, and MER, demonstrate distinct patterns and complex regulation of ligand-induced activation. J Biol Chem 2014; 289:25750-63. [PMID: 25074926].

53. Burke JM, Cao F, Irving PE, Skumatz CM. Expression of E-cadherin by human retinal pigment epithelium: delayed expression in vitro. Invest Ophthalmol Vis Sci 1999; 40:2963-70. [PMID: 10549658].

54. Mendez MG, Kojima S, Goldman RD. Vimentin induces changes in cell shape, motility, and adhesion during the epithelial to mesenchymal transition. FASEB J 2010; 24:1838-51. [PMID: 20097873].

55. Dey A, Li W. Cell cycle-independent induction of D1 and D2 cyclin expression, but not cyclin-Cdk complex formation or Rb phosphorylation, by IFNgamma in macrophages. Biochim Biophys Acta 2000; 1497:135-47. [PMID: 10838167].

56. Adijanto J, Castorino JJ, Wang ZX, Maminishkis A, Grunwald GB, Philp NJ. Microphthalmia-associated transcription factor (MITF) promotes differentiation of human retinal pigment epithelium (RPE) by regulating microRNAs-204/211 expression. J Biol Chem 2012; 287:20491-503. [PMID: 22523078].

57. Holtrich U, Wolf G, Brauninger A, Karn T, Bohme B, Rubsamen-Waigmann H, Strebhardt K. Induction and down-regulation of PLK, a human serine/threonine kinase expressed in proliferating cells and tumors. Proc Natl Acad Sci USA 1994; 91:1736-40. [PMID: 8127874].

58. He J, Choe S, Walker R, Di Marzio P, Morgan DO, Landau NR. Human immunodeficiency virus type 1 viral protein R (Vpr) arrests cells in the G2 phase of the cell cycle by inhibiting p34cdc2 activity. J Virol 1995; 69:6705-11. [PMID: 7474080].

59. Bolanos-Garcia VM, Blundell TL. BUB1 and BUBR1: multifaceted kinases of the cell cycle. Trends Biochem Sci 2011; 36:141-50. [PMID: 20888775].

60. Sharma RK, Orr WE, Schmitt AD, Johnson DA. A functional profile of gene expression in ARPE-19 cells. BMC Ophthalmol 2005; 5:25-[PMID: 16262907].

61. Westenskow PD, Moreno SK, Krohne TU, Kurihara T, Zhu S, Zhang ZN, Zhao T, Xu Y, Ding S, Friedlander M. Using flow cytometry to compare the dynamics of photoreceptor outer segment phagocytosis in iPS-derived RPE cells. Invest Ophthalmol Vis Sci 2012; 53:6282-90. [PMID: 22871841].

62. Stockinger A, Eger A, Wolf J, Beug H, Foisner R. E-cadherin regulates cell growth by modulating proliferation-dependent beta-catenin transcriptional activity. J Cell Biol 2001; 154:1185-96. [PMID: 11564756].

63. Halbleib JM, Nelson WJ. Cadherins in development: cell adhesion, sorting, and tissue morphogenesis. Genes Dev 2006; 20:3199-214. [PMID: 17158740].

64. Sprecher E, Bergman R, Richard G, Lurie R, Shalev S, Petronius D, Shalata A, Anbinder Y, Leibu R, Perlman I, Cohen N, Szargel R. Hypotrichosis with juvenile macular dystrophy is caused by a mutation in CDH3, encoding P-cadherin. Nat Genet 2001; 29:134-6. [PMID: 11544476].

65. Burke JM. Epithelial phenotype and the RPE: is the answer blowing in the Wnt? Prog Retin Eye Res 2008; 27:579-95. [PMID: 18775790].

66. Lee J, Ko M, Joo CK. Rho plays a key role in TGF-beta1-induced cytoskeletal rearrangement in human retinal pigment epithelium. J Cell Physiol 2008; 216:520-6. [PMID: 18314880].

67. Li H, Wang H, Wang F, Gu Q, Xu X. Snail involves in the transforming growth factor beta1-mediated epithelial-mesenchymal transition of retinal pigment epithelial cells. PLoS One 2011; 6:e23322-[PMID: 21853110].

68. Rizzolo LJ. Development and role of tight junctions in the retinal pigment epithelium. Int Rev Cytol 2007; 258:195-234. [PMID: 17338922].

69. Furuse M, Furuse K, Sasaki H, Tsukita S. Conversion of zonulae occludentes from tight to leaky strand type by introducing claudin-2 into Madin-Darby canine kidney I cells. J Cell Biol 2001; 153:263-72. [PMID: 11309408].

70. Van Itallie CM, Fanning AS, Anderson JM. Reversal of charge selectivity in cation or anion-selective epithelial lines by expression of different claudins. Am J Physiol Renal Physiol 2003; 285:F1078-84. [PMID: 13129853].

71. Peng S, Wang SB, Singh D, Zhao PY, Davis K, Chen B, Adelman RA, Rizzolo LJ. Claudin-3 and claudin-19 partially restore native phenotype to ARPE-19 cells via effects on tight junctions and gene expression. Exp Eye Res 2016; 151:179-89. [PMID: 27593915].

72. Boulton M, Rozanowska M, Rozanowski B. Retinal photodamage. J Photochem Photobiol B 2001; 64:144-61. [PMID: 11744401].

73. Seagle BL, Rezai KA, Kobori Y, Gasyna EM, Rezaei KA, Norris JR Jr. Melanin photoprotection in the human retinal pigment epithelium and its correlation with light-induced cell apoptosis. Proc Natl Acad Sci USA 2005; 102:8978-83. [PMID: 15951427].

74. Gamm DM, Melvan JN, Shearer RL, Pinilla I, Sabat G, Svendsen CN, Wright LS. A novel serum-free method for culturing human prenatal retinal pigment epithelial cells. Invest Ophthalmol Vis Sci 2008; 49:788-99. [PMID: 18235029].

75. Turowski P, Adamson P, Sathia J, Zhang JJ, Moss SE, Aylward GW, Hayes MJ, Kanuga N, Greenwood J. Basement membrane-dependent modification of phenotype and gene expression in human retinal pigment epithelial ARPE-19 cells. Invest Ophthalmol Vis Sci 2004; 45:2786-94. [PMID: 15277505].

76. Stanzel BV, Espana EM, Grueterich M, Kawakita T, Parel JM, Tseng SC, Binder S. Amniotic membrane maintains the phenotype of rabbit retinal pigment epithelial cells in culture. Exp Eye Res 2005; 80:103-12. [PMID: 15652531].

77. Jin M, Li S, Moghrabi WN, Sun H, Travis GH. Rpe65 is the retinoid isomerase in bovine retinal pigment epithelium. Cell 2005; 122:449-59. [PMID: 16096063].

78. Moiseyev G, Chen Y, Takahashi Y, Wu BX, Ma JX. RPE65 is the isomerohydrolase in the retinoid visual cycle. Proc Natl Acad Sci USA 2005; 102:12413-8. [PMID: 16116091].

79. Redmond TM, Poliakov E, Yu S, Tsai JY, Lu Z, Gentleman S. Mutation of key residues of RPE65 abolishes its enzymatic role as isomerohydrolase in the visual cycle. Proc Natl Acad Sci USA 2005; 102:13658-63. [PMID: 16150724].

80. Marmorstein AD, Kinnick TR. Focus on molecules: bestrophin (best-1). Exp Eye Res 2007; 85:423-4. [PMID: 16720022].

81. Hu J, Bok D. The use of cultured human fetal retinal pigment epithelium in studies of the classical retinoid visual cycle and retinoid-based disease processes. Exp Eye Res 2014; 126:46-50. [PMID: 24060345].

82. Ruiz A, Ghyselinck NB, Mata N, Nusinowitz S, Lloyd M, Dennefeld C, Chambon P, Bok D. Somatic ablation of the Lrat gene in the mouse retinal pigment epithelium drastically reduces its retinoid storage. Invest Ophthalmol Vis Sci 2007; 48:5377-87. [PMID: 18055784].

83. Batten ML, Imanishi Y, Maeda T, Tu DC, Moise AR, Bronson D, Possin D, Van Gelder RN, Baehr W, Palczewski K. Lecithin-retinol acyltransferase is essential for accumulation of all-trans-retinyl esters in the eye and in the liver. J Biol Chem 2004; 279:10422-32. [PMID: 14684738].

84. Mazzoni F, Safa H, Finnemann SC. Understanding photoreceptor outer segment phagocytosis: use and utility of RPE cells in culture. Exp Eye Res 2014; 126:51-60. [PMID: 24780752].

85. Nandrot EF, Kim Y, Brodie SE, Huang X, Sheppard D, Finnemann SC. Loss of synchronized retinal phagocytosis and age-related blindness in mice lacking alphavbeta5 integrin. J Exp Med 2004; 200:1539-45. [PMID: 15596525].

86. Nandrot E, Dufour EM, Provost AC, Pequignot MO, Bonnel S, Gogat K, Marchant D, Rouillac C, Sepulchre de Conde B, Bihoreau MT, Shaver C, Dufier JL, Marsac C, Lathrop M, Menasche M, Abitbol MM. Homozygous deletion in the coding sequence of the c-mer gene in RCS rats unravels general mechanisms of physiological cell adhesion and apoptosis. Neurobiol Dis 2000; 7:6 Pt B586-99. [PMID: 11114258].

87. D'Cruz PM, Yasumura D, Weir J, Matthes MT, Abderrahim H, LaVail MM, Vollrath D. Mutation of the receptor tyrosine kinase gene Mertk in the retinal dystrophic RCS rat. Hum Mol Genet 2000; 9:645-51. [PMID: 10699188].

88. Finnemann SC. Focal adhesion kinase signaling promotes phagocytosis of integrin-bound photoreceptors. EMBO J 2003; 22:4143-54. [PMID: 12912913].

89. Mansky KC, Sulzbacher S, Purdom G, Nelsen L, Hume DA, Rehli M, Ostrowski MC. The microphthalmia transcription factor and the related helix-loop-helix zipper factors TFE-3 and TFE-C collaborate to activate the tartrate-resistant acid phosphatase promoter. J Leukoc Biol 2002; 71:304-10. [PMID: 11818452].

90. Masuda T, Esumi N. SOX9, through interaction with microphthalmia-associated transcription factor (MITF) and OTX2, regulates BEST1 expression in the retinal pigment epithelium. J Biol Chem 2010; 285:26933-44. [PMID: 20530484].

91. Hu G, Huang K, Yu J, Gopalakrishna-Pillai S, Kong J, Xu H, Liu Z, Zhang K, Xu J, Luo Y, Li S, Sun YE, Iverson LE, Xue Z, Fan G. Identification of miRNA signatures during the differentiation of hESCs into retinal pigment epithelial cells. PLoS One 2012; 7:e37224-[PMID: 22848339].

92. Ohana R, Weiman-Kelman B, Raviv S, Tamm ER, Pasmanik-Chor M, Rinon A, Netanely D, Shamir R, Solomon AS, Ashery-Padan R. MicroRNAs are essential for differentiation of the retinal pigmented epithelium and maturation of adjacent photoreceptors. Development 2015; 142:2487-98. [PMID: 26062936].

93. Kutty RK, Samuel W, Jaworski C, Duncan T, Nagineni CN, Raghavachari N, Wiggert B, Redmond TM. MicroRNA expression in human retinal pigment epithelial (ARPE-19) cells: increased expression of microRNA-9 by N-(4-hydroxyphenyl)retinamide. Mol Vis 2010; 16:1475-86. [PMID: 20806079].

94. Zhao C, Yasumura D, Li X, Matthes M, Lloyd M, Nielsen G, Ahern K, Snyder M, Bok D, Dunaief JL, LaVail MM, Vollrath D. mTOR-mediated dedifferentiation of the retinal pigment epithelium initiates photoreceptor degeneration in mice. J Clin Invest 2011; 121:369-83. [PMID: 21135502].

95. Rizzolo LJ, Chen X, Weitzman M, Sun R, Zhang H. Analysis of the RPE transcriptome reveals dynamic changes during the development of the outer blood-retinal barrier. Mol Vis 2007; 13:1259-73. [PMID: 17679949].

Articles are provided courtesy of Emory University and the Zhongshan Ophthalmic Center, Sun Yat-sen University, P.R. China. The print version of this article was created on 5 March 2017. This reflects all typographical corrections and errata to the article through that date. Details of any changes may be found in the online version of the article.